Geol. Mag. **151** (*5*), *2014, pp. 830–849.* © *Cambridge University Press 2013*
doi:10.1017/S0016756813000897

Carbon isotope signatures of pedogenic carbonates from SE China: rapid atmospheric pCO_2 changes during middle–late Early Cretaceous time

XIANGHUI LI*†, HUGH C. JENKYNS‡§, CHAOKAI ZHANG*, YIN WANG¶, LING LIU¶ & KE CAO‖

*State Key Laboratory of Mineral Deposit Research, School of Earth Sciences and Engineering Nanjing University, Nanjing 210093, China
†State Key Laboratory of Oil–Gas Reservoir Geology and Exploitation, Chengdu University of Technology, Chengdu 610059, China
‡Department of Earth Sciences, University of Oxford, South Parks Road, Oxford OX1 3AN, UK
¶East China Mineral Exploration and Development Bureau of Jiangsu Province, Nanjing 210007, China
‖Qingdao Institute of Marine Geology, Qingdao 200092, China

(*Received* 6 July 2012; *accepted* 24 September 2013; *first published online* 20 November 2013)

Abstract – Lower Cretaceous pedogenic carbonates exposed in SE China have been dated by U–Pb isotope measurements on single zircons taken from intercalated volcanic rocks, and the ages integrated with existing stratigraphy. $\delta^{13}C$ values of calcretes range from –7.0 ‰ to –3.0 ‰ and can be grouped into five episodes of increasing–decreasing values. The carbon isotope proxy derived from these palaeosol carbonates suggests pCO_2 mostly in the range 1000–2000 parts per million by volume (ppmV) at $S(z)$ (CO_2 contributed by soil respiration) = 2500 ppmV and 25 °C during the Hauterivian–Albian interval (*c.* 30 Ma duration). Such atmospheric CO_2 levels are 4–8 times pre-industrial values, almost double those estimated by geochemical modelling and much higher than those established from stomatal indices in fossil plants. Rapid rises in pCO_2 are identified for early Hauterivian, middle Barremian, late Aptian, early Albian and middle Albian time, and rapid falls for intervening periods. These episodic cyclic changes in pCO_2 are not attributed to local tectonism and volcanism but rather to global changes. The relationship between reconstructed pCO_2 and the development of large igneous provinces (LIPs) remains unclear, although large-scale extrusion of basalt may well be responsible for relatively high atmospheric levels of this greenhouse gas. Suggested levels of relatively low pCO_2 correspond in timing to intervals of regional to global enrichment of marine carbon in sediments and negative carbon isotope ($\delta^{13}C$) excursions characteristic of the oceanic anoxic events OAE1a (Selli Event), Kilian and Paquier events (constituting part of the OAE 1b cluster) and OAE1d. Short-term episodes of high pCO_2 coincide with negligible carbon isotope excursions associated with the Faraoni Event and the Jacob Event. Given that episodes of regional organic carbon burial would draw down CO_2 and negative $\delta^{13}C$ excursions indicate the addition of isotopically light carbon to the ocean–atmosphere system, controls on the carbon cycle in controlling pCO_2 during Early Cretaceous time were clearly complex and made more so by atmospheric composition also being affected by changes in silicate weathering intensity.

Keywords: atmospheric CO_2, pedogenic calcrete, Early Cretaceous, SE China.

1. Introduction

To understand how the Earth behaves under greenhouse conditions, the study of Cretaceous palaeoclimates has proven useful. Reconstruction of Cretaceous pCO_2 has been attempted using techniques such as determination of stomatal indices of fossil cuticle (e.g. Beerling, McElwain & Osborne, 1998; Retallack, 2001; Beerling & Royer, 2002; Beerling & Berner, 2005; Haworth *et al.* 2005), organic geochemistry (Sinninghe Damsté *et al.* 2008), study of carbon isotope composition of calcium carbonate in ancient soils (e.g. Cerling, 1991; Ekart *et al.* 1999; Robinson *et al.* 2002; Retallack, 2005, 2009) and geochemical modelling (e.g. Berner, 1994, 2001, 2006; Tajika, 1999; Wallmann, 2001; François, Grard & Goddéris, 2005).

In the generalized models of Berner (2001, 2006) and Tajika (1999), atmospheric pCO_2 is high during latest Jurassic–earliest Cretaceous time (150–140 Ma), quickly falls during middle Early Cretaceous time (*c.* 140–130 Ma), recovers to a higher level during late Early Cretaceous time (*c.* 130–120 Ma), maintains a stable higher level through mid-Cretaceous time (*c.* 120–110 Ma) and then falls towards the end of Cretaceous time. The only difference in the Wallmann (2001) model is that atmospheric pCO_2 is reconstructed as being much lower during Early Cretaceous time. Changes in Cretaceous pCO_2 based on stomatal indices from plant cuticle are not readily comparable with one another because of the difference in stratigraphic

§Author for correspondence: hughj@earth.ox.ac.uk

resolution (Retallack, 2001; Haworth *et al.* 2005; Sun *et al*. 2007); the study of Haworth *et al*. (2005), based on cuticle from England and the United States, produces data that can, however, be compared with results from pedogenic carbonate from the same sedimentary unit in England. Estimates of pCO_2, primarily based on study of pedogenic carbonate from localities worldwide, match more closely the earlier model of Berner (1994) in terms of absolute values than the later models (Berner, 2001, 2006), although the trends are broadly similar. In summary, Cretaceous pCO_2 is considered to have been on average 4–8 times higher than pre-industrial values; some reconstructions show little variation on a scale of tens of millions of years, while others show significant short-term excursions.

However, three major problems persist: (1) the pCO_2 pedogenic carbonate palaeobarometer typically yields much higher values than do fossil stomata (Royer, 2006; Fletcher *et al.* 2008); (2) the exact intervals to which the ancient pCO_2 determinations apply are commonly only approximate because, in the absence of unambiguous palaeomagnetic reversals (cf. Nordt, Atchley & Dworkin, 2002, 2003), stratigraphy is compromised by the common lack of age-diagnostic taxa in continental lithofacies; and (3) (following from (2)) the lack of high-resolution data precludes correlation of movements in pCO_2 with changes in the global carbon cycle derived from marine sediments. The first problem may be addressed by using more realistic constraints on the assumed concentrations of soil CO_2 (Breecker, Sharp & McFadden, 2010); the second and third problem can be overcome by finding pedogenic carbonates that can be accurately dated.

There is little in the way of pCO_2 reconstructions from Chinese sequences and all those investigated to date suffer from the stratigraphic limitations that beset continental sediments: the investigated material includes two mid-Cretaceous palaeosols from the Lhasa terrane in Tibet (Leier *et al.* 2009), Lower Cretaceous palaeosols in southwestern China (Huang, Retallack & Wang, 2012) and fossil *Ginkgo* leaves from the lowermost Cretaceous of north China that have yielded stomatal indices (Sun *et al*. 2007). However, Jurassic–Cretaceous continental sediments are widespread in mainland China and offer potential for this type of investigation. In this work, we present new carbon isotope data from well-dated pedogenic carbonates cropping out in Zhejiang and Jiangxi, SE China (Fig. 1), and estimate atmospheric pCO_2 during middle–late Early Cretaceous time. Furthermore, we endeavour to explore the linkages between changes in atmospheric pCO_2 and large-scale geological events that may have affected the global carbon cycle.

2. Geological setting

A number of Cretaceous continental sedimentary basins were formed by regional extension during late Mesozoic tectonic events in east and SE Asia (e.g. Liu, 1982; Ren, 1990; Okada, 1999; Shu *et al.* 2008, 2009); those in SE China are of relatively small sizes, typically several hundred square kilometres but ranging up to *c.* 3000 km^2 for a single basin (Ren & Chen, 1989; Yu *et al.* 2003; Shu *et al.* 2009). Moving from east to west in South China, the continental sedimentary basins are dominated by volcanic rocks, passing to sediments interbedded with volcanic rocks, in turn passing to predominantly sedimentary successions (e.g. Li, Shen & Wang, 1987; Lu, Zhu & Qin, 2000; Chen *et al.* 2005; Shu *et al.* 2009) (Fig. 1). We chose to investigate sequences with interbedded volcanic and sedimentary rocks because they provide the opportunity to determine more closely the age of the samples.

In this area, argillisols, calcisols and oxisols are the typical pedogenic sediments and were mostly developed during mid-Cretaceous time under inferred arid to semi-arid climatic conditions (Li *et al.* 2009). The argillisols are characterized by burrow and root traces within reddish silty mudrock, the calcisols comprise pedogenic carbonate concretions in pale-purple calcareous mudrock and the oxisols are an association of ferric oxide coatings and concretions within reddish-purple to greyish-orange siltstone and mudrock. Calcisols are interpreted as having formed in fluvial floodplain deposits and marginal lacustrine environments. The palaeosol and calcretes primarily occur in the Jiande Group, Yongkang Group, Qujiang Group in the basins of western Zhejiang and Shixi and Luotang Formations in the basins of NE Jiangxi. The Jiande Group comprises the Laocun, Huangjian, Shouchang and Hengshan Formations, the Yongkang Group is composed of the Guantou, Chaochuan and Fangyan Formations and the Qujiang Group consists of the Zhongdai, Jinhua and Quxian Formations. All these units are generally attributed to the Lower Cretaceous (e.g. Cao, 1986; Zheng, 1993; Shou, 1995; Yu & Xu, 1999; Chen *et al.* 2006, 2008).

To date, the stratigraphic organization and age assignment of strata in these basins has been problematic due to the presence of many local lithostratigraphic units compounded by a lack of datable material in different basins (Yu *et al.* 2003). Fossils of stratigraphic use are few and far between, and changes in lithofacies have led to different classifications and correlation of complicated lithostratigraphic units in SE China. Some palaeontological studies of plants, spores, bivalves, ostracods and dinosaurs have been undertaken (e.g. Cao, 1986; Zheng, 1993; Shou, 1995; Chen *et al.* 2006), as have palaeomagnetic stratigraphy (Hu, Li & Ma, 1990; Liu *et al.* 1992; Morinaga, Inokuchi & Miyata, 1999) and isotope chronology of volcanic and plutonic rocks (e.g. Hu *et al.* 1982; Li, Shen & Wang, 1989; Yu & Xu, 1999; Chen *et al.* 2008). However, the strata are not yet well constrained in terms of age.

3. Sample dating

In this study, concretionary pedogenic carbonates were sampled within calcisols in seven locations (Fig. 1) from seven different formations: Chaochuan, Guantou,

https://doi.org/10.1017/S0016756813000897 Published online by Cambridge University Press

Table 1. Description of volcanic rocks from western Zhejiang, SE China and absolute ages of single zircon U–Pb isotopes

Sample	Section	Location	GPS (°N, °E)	Lithology	Age (Ma)	Error (Ma)	Error (%)	MSWD	Zircon number
0126–02ZK	4	Yongkang	284709.6, 1200437.4	Dacitic crystal tuff	123.2	1.2	1.0	0.32	13
0127–01ZK	4	Yongkang	284753.6, 1200539.4	Vitric-crystal tuff	117.3	1.9	1.6	1.20	10
0127–10ZK	4	Yongkang	284815.1, 1200621.6	Dacitic vitric-crystal tuff	113.1	1.2	1.1	1.16	15
0128–02ZK	1	Jiande	292439.4, 1190919.6	Dacitic crystal tuff	132.3	1.6	1.2	1.50	13
0128–04ZK	1	Jiande	292429.2, 1190937.2	Dacitic crystal tuff	130.3	3.3	2.5	4.30	10
ZC-06ZK	1	Jiande	292313.1, 1191049.9	Tuff	125.0	1.0	0.8	0.00	15
LZ2–17ZK	5	Lishui	283237.6, 1194502.2	Vitric tuff	115.3	1.5	1.3	1.17	15
1103–03ZK	5	Lishui	283215.7, 1194523.3	Crystal tuff	107.1	1.7	1.6	1.4	11

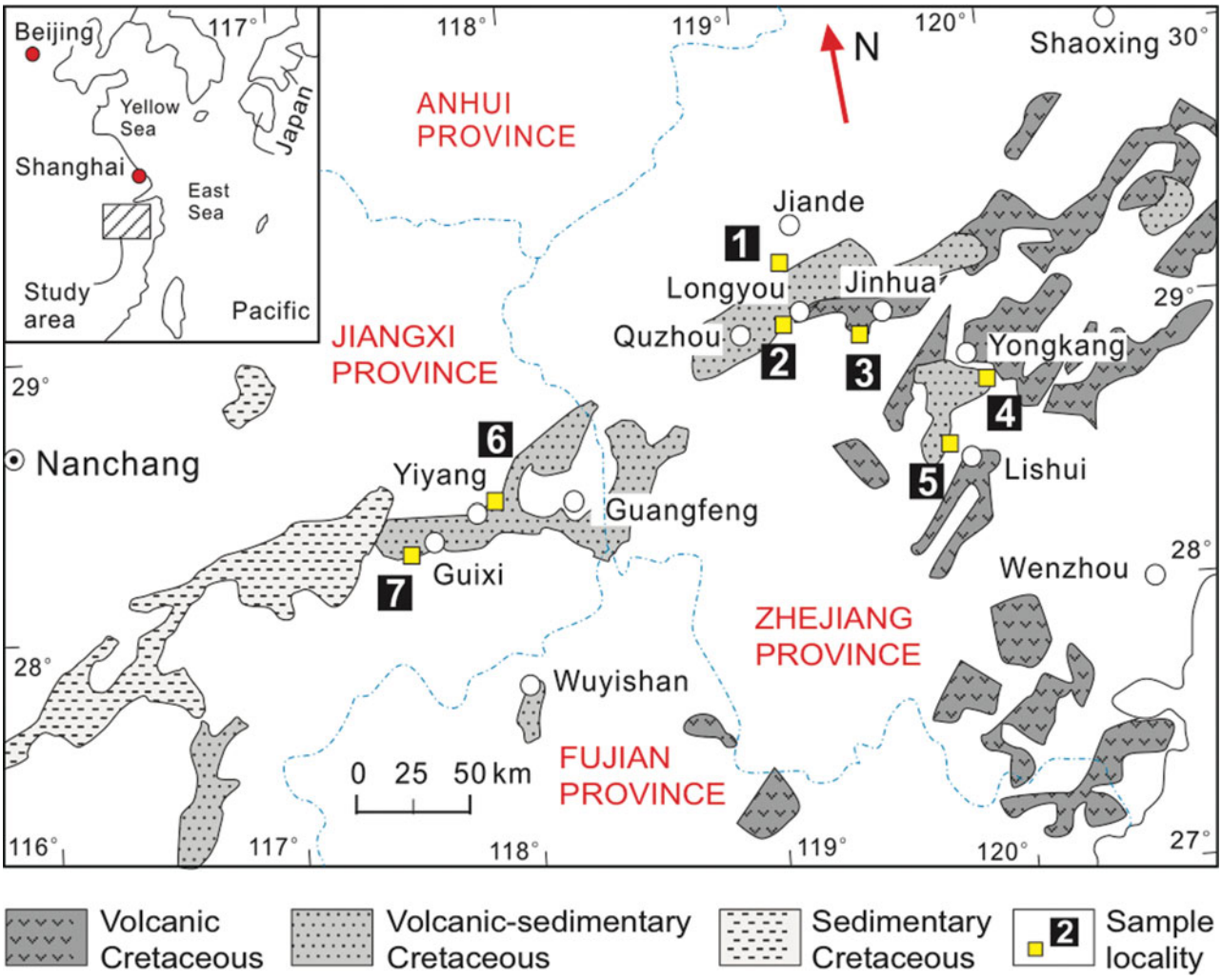

Figure 1. (Colour online) Sketch map of Cretaceous outcrops in SE China, simplified after Shu *et al.* (2009). The squares are the sample localities and the numbers in white in black squares indicate sample locations: (1) Tongjia to Yanxia, Jiande; (2) Gaoxiantang, Longyou; (3) Zhongdai, Jinhua; (4) Guantou to Fenglin, Yongkang; (5) Laozhu, Lishui; (6) Huobashan, Yiyang; and (7) Xintian, Guixi. Sections 1–5 are located in Zhejiang province and sections 6–7 are located in Jiangxi province.

Jinhua, Laocun, Luotang, Shixi and Zhongdai Formations (Fig. 2). In the past, these formations were often described in general terms as either Early or late Early Cretaceous in age.

To improve the age control of the sequences, samples of the intercalated volcanic rocks were taken for single zircon U–Pb isotope analyses (Table 1, Fig. 2) and the results combined with newly published U–Pb zircon data (Li *et al.* 2011) as well as with other published isotope ages where appropriate (Table S1, available at http://journals.cambridge.org/geo; Fig. 2). In this work and Li *et al.* (2011), zircon U–Pb isotopic measurements (10–15 single zircons for each sample) were completed by laser ablation inductively coupled plasma mass spectrometry (LA-ICP-MS) at the State Key Laboratory for Mineral Deposits Research, Nanjing University following methods described by Jackson *et al.* (2004). Analyses of

https://doi.org/10.1017/S0016756813000897 Published online by Cambridge University Press

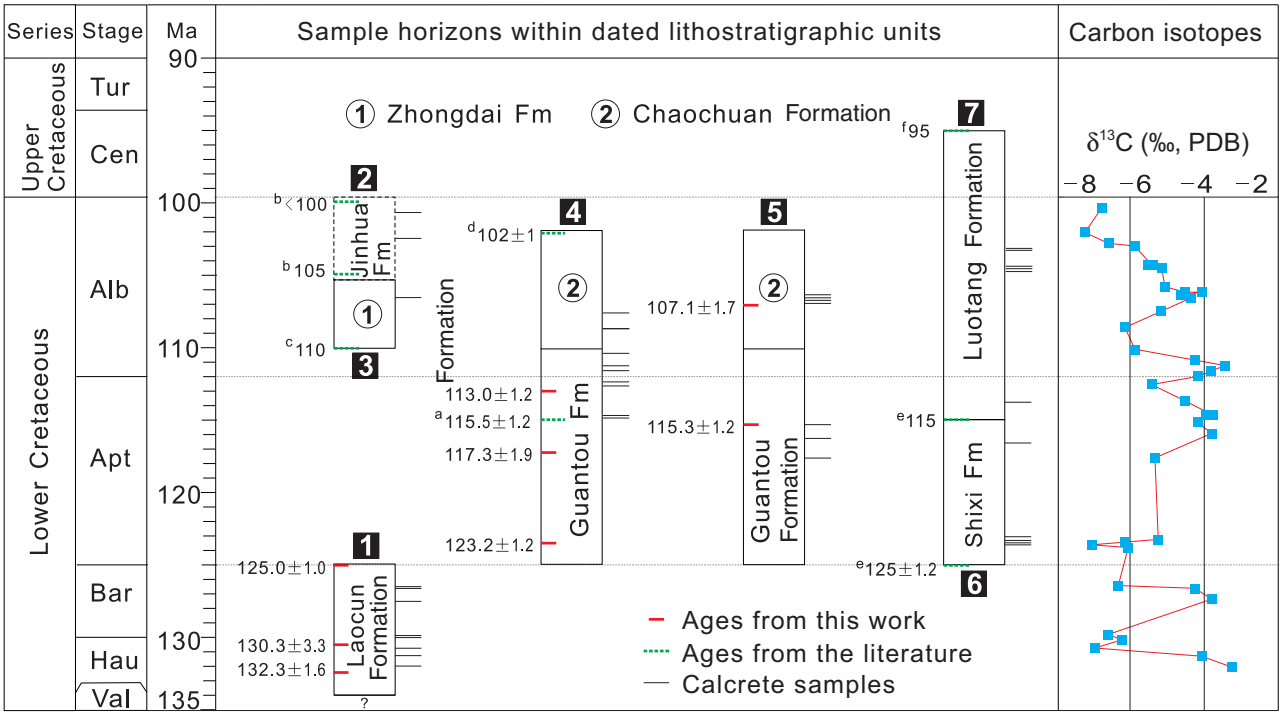

Figure 2. (Colour online) Diagram showing the Cretaceous stratigraphy in SE China with sample horizons of pedogenic carbonate calcretes and changes in carbon isotope values. The ages of samples were assigned by absolute-age positions of volcanically derived zircons (this work) and from minerals and rocks studied by other workers. The numbers in black squares represent the sample locations referred to in Figure 1. Short lines to the right of the rectangles (lithostratigraphic units) are the horizons of calcrete samples. Short bars within rectangles indicate the positions of the volcanic horizons, giving the newly determined U–Pb isotope and other isotope absolute ages. Those age numbers with superscript letters are the ages cited from: (a) Li *et al.* (2011); (b) Zhang (1987); (c) TRGZ (1992); (d) Xing *et al.* (2008); (e) Wang *et al.* (2002); (f) Xing *et al.* (2008) and inferred (see text). These dates were chosen to estimate the ages of calcrete samples from the assigned ages at the top and bottom of key formations. More details are given in Table 2.

Mud Tank zircon as an unknown yielded a weighted $^{206}Pb/^{238}U$ age of 720 ± 12 Ma – 736 ± 6 Ma (2σ) for the standard samples, which is in good agreement with the recommended value (thermal ionization mass spectrometry or TIMS age = 732 ± 5 Ma; Black & Gulson, 1978). Analytical results and relevant isotopic rates were calculated using GLITTER 4.4 (van Achterbergh *et al.* 2001). Common Pb corrections were carried out using the method described by Andersen (2002). The concordant results are mainly <2.0 % in error and <1.5 in mean square weighted distribution (MSWD; Table 1). The new results combined with extant data allow the sedimentary formations containing pedogenic calcrete to be better constrained than previously in terms of age (Fig. 2).

Calcrete sample ages were estimated by interpolation: $A = B - \gamma \times C$ where A is the estimated age of a calcrete sample, B is the nearest isotopic age of an intercalated volcanic rock below, C is the thickness of the sediment to that same volcanic rock and γ is the ratio of age to thickness between the nearest absolute ages of volcanic rocks sampled above and below the pedogenic carbonate in question. All sample ages are estimated and listed in supplementary materials (Table S1, available at http://journals.cambridge.org/geo) and can be read from Figure 2.

The Laocun Formation comprises volcanic rocks interbedded with sedimentary rocks, and was relatively easy to date in the past. The isotopes derived from sanidine and biotite by Ar–K, Ar–Ar and Rb–Sr methods show an age range between 135 Ma and 127 Ma (Yu & Xu, 1999). In this work, zircon U–Pb dating of volcanic single zircons mostly indicates a range of *c.* 132.13 ± 1.6 Ma – 125.0 ± 1.0 Ma (Table 1, Fig. 2). The new isotopic dating allows the calcrete samples to be relatively well constrained in age.

The Guantou Formation mainly comprises varicoloured (tuffaceous) mudrocks with intercalations of tuff, and is robustly confined between 123.0 ± 1.2 Ma and 113.0 ± 1.2 Ma by the new zircon U–Pb dating presented in this work. Considering other isotope ages (Li *et al.* 2011) and the positions of volcanic samples (Table S1, available at http://journals.cambridge.org/geo), it is suggested that the formation ranges from 125.0 Ma to 110.0 Ma (Fig. 2). Correspondingly, the overlying Chaochuan Formation, comprising reddish siltstone and mudrock with intercalated sandstone, was adjusted to give a duration of 110.0 Ma to *c.* 102.0 Ma by the age limits of the underlying Guantou Formation and the 102.0 ± 1.0 Ma Rb–Sr isotope age of an ignimbrite (Xing *et al.* 2008) at the top of the Chaochuan Formation.

https://doi.org/10.1017/S0016756813000897 Published online by Cambridge University Press

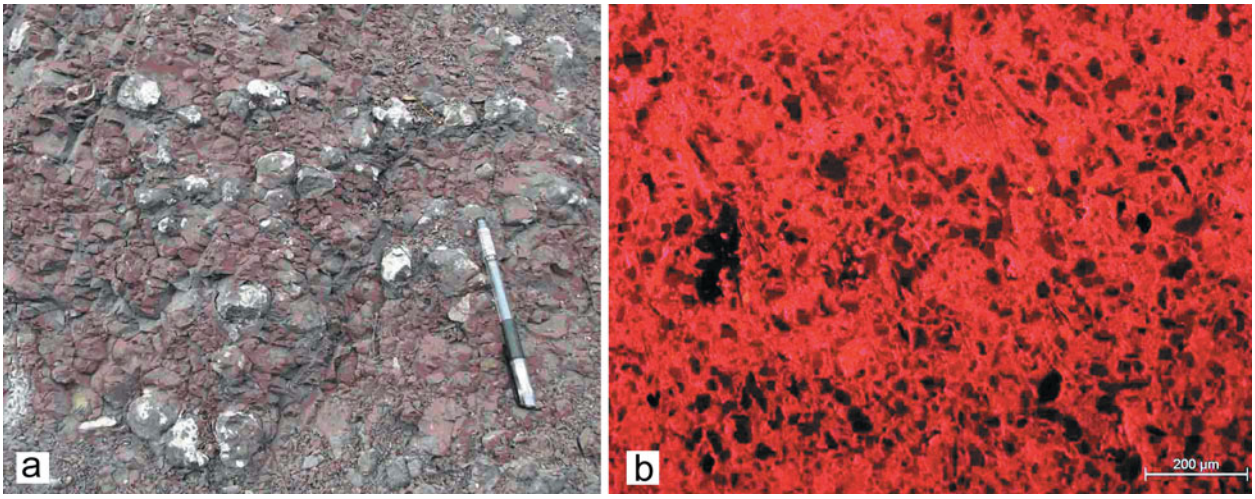

Figure 3. (Colour online) (a) Field photo showing the pedogenic calcretes. Sample 0127-02, Upper Guantou Formation at section 4, northern Guantou village of Yongkang county, Zhejiang province. Pen is 15 cm long. (b) Cathodoluminescence micrograph showing evenly distributed salmon-red colour of micritic calcite in calcrete, indicating little diagenetic alteration. Dark-grey and black non-luminescent areas indicate non-carbonates (quartz, lithic fragments and feldspar as well as other opaques). Sample 1109-01, upper 42nd bed of the Luotang Formation, Wanghua village of Guixi county, Jiangxi province.

The Zhongdai Formation is characterized by a succession of coarse to fine terrigenous sediment with basalt intercalations. The dinosaur fossil *Chilantaisaurus zhejiangensis* (PGSZ, 1979) and K–Ar isotope ages of basalt indicate that the formation is of late Early Cretaceous age (Zhang, 1987; TRGZ, 1992). The calcrete sample is roughly constrained to date between 110.0 ± 1.9 Ma (TRGZ, 1992) and 105.0 ± 1.7 Ma (Zhang, 1987), and is estimated as *c.* 106.5 Ma (Table S1, available at http://journals.cambridge.org/geo; Fig. 2). The Jinhua Formation consists of pale purple silty mudrock and argillaceous siltstone. It is conformable with the underlying Zhongdai Formation and the overlying Quxian Formation, indicating an age younger than *c.* 105 Ma. We used the estimated sedimentary rate (49.6 m Ma^{-1}) of the Zhongdai Formation to give an approximate age of the two sampled calcretes by reference to their positions within the Jinhua Formation (Table S1, available at http://journals.cambridge.org/geo; Fig. 2) since both formations developed in the same tectonic and sedimentary setting.

The Shixi Formation in eastern Jiangxi province is composed of sandstone interbedded with mudrock. The underlying volcanic Ehuling Formation was dated as 137.0 ± 0.94 Ma (132–144 Ma) by U–Pb isotopes of zircons in trachyte (Liu, Wu & Liu, 2009) and indicates that the Shixi Formation was formed later than 132 Ma. Two isotopic ages have been published for the Shixi Formation: 125.0 ± 1.2 Ma (Rb–Sr isotope of dacite; Wang *et al.* 2002) and 119.2 ± 1.3 Ma (K–Ar isotope of sanidine; Li, Shen & Wang, 1989) at the lower and middle part of the section, respectively. The top of the section is estimated as 115 Ma in age. Consequently, the age of the calcrete samples was readily estimated within the formation (Table S1, available at http://journals.cambridge.org/geo; Fig. 2).

Above the Shixi Formation lies the Luotang Formation, constituted by reddish terrigenous sediment with many calcrete nodules and a few intercalations of volcanic rock. Wu (1995, 2000) suggested the Luotang Formation as Albian–Cenomanian in age based on the biota (plants, ostracods, bivalves, charophytes and conchostraca). Isotopic data gave the following ages: 119.2 ± 1.3 Ma, 101.8 ± 3.2 Ma based on K–Ar isotopes in sanidine (Li, Shen & Wang, 1989); and 98.0 ± 1.1 Ma, 91.7 ± 1.0 Ma based on K–Ar isotope ages of basalt (Wang *et al.* 2002). By combining these ages, the Luotang Formation is suggested as lasting from 115 Ma to 95 Ma. This estimate is used for calculating the ages of the calcrete samples.

4. Materials and methods

A total of 87 calcrete samples were collected *in situ* from 38 horizons (Table 1; Table S1, available at http://journals.cambridge.org/geo) at seven locations (Figs 1, 2); 2–4 calcretes from each horizon were used to measure carbon isotope ratios, and differences in carbon isotope values among single calcretes in the same horizon were determined.

Calcretes are quite readily recognized following criteria assembled by Alonso-Zarza (2003): they are typically spherical–elliptical to ginger-root shaped; they vary in size over the range 2–100 mm in length or diameter; and they represent up to 50 % of the mudrock in which they are enclosed (Fig. 3a). Calcrete fabrics are characterized by fine-grained carbonate (Fig. 3b) in the form of concentric (pisolitic) concretions and continuous multi-layered laminar coatings, solutional pipes and cavities, locally with a brecciated texture (cf. Ludvigson *et al.* 2010). Cathodoluminescence reveals an evenly textured orange to salmon-red colour (Fig. 3b), indicating homogenous precipitation of micritic calcite

https://doi.org/10.1017/S0016756813000897 Published online by Cambridge University Press

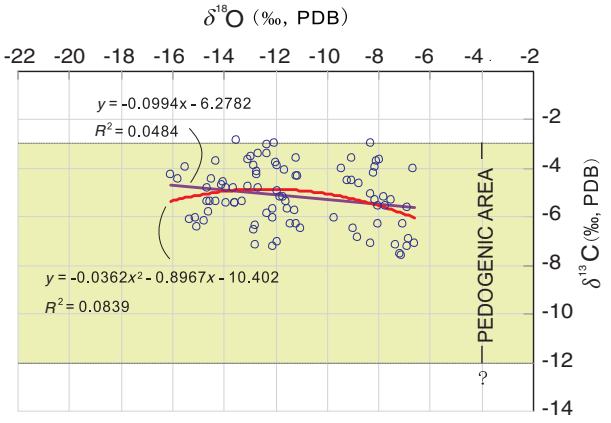

Figure 4. (Colour online) Cross-plot of carbon and oxygen isotopic values of the Lower Cretaceous pedogenic calcretes in SE China. Note the minimal covariance of $\delta^{13}C$ with $\delta^{18}O$: $R^2 = 0.05$ using binomial single regression equation and $R^2 = 0.08$ using binomial quadratic regression equation. These data indicate little diagenetic imprint on $\delta^{13}C$ values. Yellow shaded area indicates the main distribution of $\delta^{13}C$ values for globally distributed Cretaceous pedogenic calcrete.

during calcrete formation. Carbon and oxygen isotope values show little covariance with $R^2 = 0.05$ (using the binomial single equation) and $R^2 = 0.08$ (using the binomial quadratic equation), indicating that $\delta^{13}C$ and $\delta^{18}O$ values are independent of each other (Fig. 4). The uniform cathodoluminescence colour of micritic calcite, the small degree of covariance between $\delta^{13}C$ and $\delta^{18}O$ values and scanty evidence for compaction demonstrate that the micritic calcites have not been diagenetically altered in the areas chosen for drilling.

Powdered samples of 0.5–1.0 mg were drilled for isotopic analysis within strictly limited 1.0–2.0 mm diameter areas where spar-filled micro-cracks, veins and vugs were absent. The resultant powder was dried in an oven at 60 °C for 10 hours before being moved to sample vials. Carbon dioxide for isotopic analysis was released using orthophosphoric acid at 70 °C and analysed online in a Finnigan MAT 252 mass spectrometer at the Key Laboratory of Marine Geology, Tongji University. Precision was regularly checked with a Chinese national carbonate standard (GBW04405) and the international standard NBS19, and reproducibility of both $\delta^{18}O$ and $\delta^{13}C$ on standards and unknowns is within ± 0.07‰. Calibration to the international PeeDee Belemnite (PDB) scale was performed through NBS19 and NBS18 standards.

5. Model equation

The equation of Cerling (1999) was used to calculate pCO_2 in this study:

$$C_a = S(z)(\delta^{13}C_s - 1.0044\,\delta^{13}C_r - 4.4)/(\delta^{13}C_a - \delta^{13}C_s)$$

where C_a is atmospheric pCO_2; $\delta^{13}C_s$, $\delta^{13}C_r$ and $\delta^{13}C_a$ are the isotopic compositions (‰) of soil CO_2, soil-respired CO_2 and atmospheric CO_2, respectively; and $S(z)$ is the CO_2 contributed by soil respiration (in parts per million by volume or ppmV). All the parameter values used in the calculation are listed in Table 2 and Tables S3–S4 (available at http://journals.cambridge.org/geo).

As for Ekart *et al.* (1999), $\delta^{13}C_s$ was calculated from the carbon isotope composition ($\delta^{13}C_c$) of pedogenic carbonate according to the temperature-dependent fractionation factor –8.98 ‰; in this case the pCO_2 values are much lower than those used in the Romanek, Grossman & Morse (1992) formula (cf. columns 3 and 4 of Table 2). $\delta^{13}C_s$ was therefore further calibrated as $\delta^{13}C_{sc}$ by the formula of Romanek, Grossman & Morse (1992) (see Table 2; Tables S2–S3, available at http://journals.cambridge.org/geo), in which palaeotemperature is estimated as 25 °C based on palaeomagnetic data and latitude–temperature correlations (Besse & Courtillot, 1988; Ekart *et al.* 1999). An average value of –6.5 ‰ was chosen as the $\delta^{13}C_a$ for the mid-Cretaceous (*c.* 130–95 Ma) soil-respired CO_2 (e.g. Ekart *et al.* 1999; Lee *et al.* 1999; Lee & Hisada, 1999; Robinson *et al.* 2002; Leier *et al.* 2009) and the $\delta^{13}C_a$ was generally calibrated as $\delta^{13}C_{ac}$ from $\delta^{13}C_r$ (see below) of soil-respired CO_2 using the Arens, Jahren & Amundson (2000) relation: $(\delta^{13}C_r + 18.67)/1.1$.

$\delta^{13}C_r$ represents average bulk C3 vascular land-plant tissue (Arens, Jahren & Amundson, 2000), reflecting atmospheric $\delta^{13}CO_2$ linearly across pCO_2 levels (Jahren *et al.* 2001; Jahren, Arens & Harbeson, 2008). As indicated by Ekart *et al.* (1999), some degree of error in pCO_2 reconstructions would result if $\delta^{13}C_r$ changed from –23.5 to –24.3 ‰. However, the possible errors (at most 10 %, generally <5 %) do not significantly influence the trend of the result. The $\delta^{13}C_{om}$ (carbon isotope ratio of soil organic matter based on the range of modern C3 ecosystem fractionations; Buchmann *et al.* 1998; Ekart *et al.* 1999) of organic matter within palaeosols is commonly thought to be representative of $\delta^{13}C_r$ in the model equation (Cerling, 1999), and values through the Phanerozoic can be read from the model curve of Ekart *et al.* (1999). The $\delta^{13}C_{om}$ (i.e. $\delta^{13}C_r$) varies between –23.5 and –24.3 ‰ for the middle–late Early Cretaceous interval; details are given in column 6 of Table 2 and supplementary materials (Tables S2–S4, available at http://journals.cambridge.org/geo).

However, the model curve of Ekart *et al.* (1999) is a highly smoothed average, designed for very long-term (tens to hundreds of millions of years) reconstructions and does not capture the variability in $\delta^{13}C$ of the ocean–atmosphere carbon reservoir on shorter time scales such as those investigated here. We therefore also used the Early Cretaceous $\delta^{13}C$ curve (Fig. 5b) of biostratigraphically well-dated hemipelagic sediments from northern Tethys (SE France) for an estimate of $\delta^{13}C_r$. Firstly, we read the $\delta^{13}C_{oc}$ (marine calcite) value corresponding to the age point of samples in this work, and made a calculation using a –26 ‰ fractionation factor between pelagic carbonate and soil organic matter (Ekart *et al.* 1999). The $\delta^{13}C_{roc}$ (column 7 of Table 2) of soil-respired CO_2 obtained in this way yielded values of –22.4 to –24.8 ‰ (mostly −23.5 to −24.6 ‰),

https://doi.org/10.1017/S0016756813000897 Published online by Cambridge University Press

Table 2. Comparative estimates of middle–late Early Cretaceous pCO_2 at different time horizons

		Time horizon (see table footnotes 1–16)															
Sample	Age (Ma)	1 $\delta^{13}C_c$	2 $\delta^{13}C_{oc}$	3 $\delta^{13}C_s$	4 $\delta^{13}C_{sc}$	5 $\delta^{13}C_r$	6 $\delta^{13}C_{ac}$	7 $\delta^{13}C_{roc}$	8 $\delta^{13}C_{aoc}$	9 pCO_2	10 pCO_2	11 pCO_2	12 pCO_2	13 pCO_2	14 pCO_2	15 pCO_2	16 pCO_2
GX-06A	100.8	– 6.82	1.94	– 15.80	– 15.66	– 24.1	– 4.94	– 24.1	– 4.90	2154	1934	1077	1132	922	967	954	– 13
GX-04A	102.4	– 7.27	2.08	– 16.25	– 16.11	– 24.0	– 4.85	– 23.9	– 4.77	1772	1599	886	937	758	799	776	– 23
1109–02A	103.1	– 6.68	1.97	– 15.66	– 15.52	– 23.9	– 4.75	– 24.0	– 4.87	2153	1897	1077	1132	904	948	990	41
1109–01A	103.3	– 5.94	1.79	– 14.92	– 14.79	– 23.9	– 4.75	– 24.2	– 5.04	2782	2401	1391	1453	1152	1201	1315	115
1108–06A	104.6	– 5.43	1.71	– 14.41	– 14.28	– 23.8	– 4.66	– 24.3	– 5.11	3220	2715	1610	1678	1307	1358	1558	200
1108–07A	104.7	– 5.56	1.90	– 14.54	– 14.41	– 23.8	– 4.66	– 24.1	– 4.94	3088	2613	1544	1610	1257	1307	1424	117
1108–05A	104.8	– 5.22	1.90	– 14.20	– 14.07	– 23.8	– 4.66	– 24.1	– 4.94	3445	2886	1722	1793	1391	1443	1568	126
1103–07A	106.1	– 5.12	1.60	– 14.10	– 13.97	– 23.8	– 4.66	– 24.4	– 5.21	3556	2970	1778	1850	1432	1485	1749	264
1103–06A	106.4	– 4.55	1.99	– 13.53	– 13.41	– 23.8	– 4.66	– 24.0	– 4.85	4249	3485	2125	2205	1685	1742	1843	101
ZD-04A	106.5	– 4.07	1.99	– 13.05	– 12.93	– 23.8	– 4.66	– 24.0	– 4.85	4927	3973	2464	2553	1924	1986	2099	112
1103–05A	106.6	– 4.66	1.82	– 13.64	– 13.52	– 23.8	– 4.66	– 24.2	– 5.01	4107	3380	2053	2132	1633	1690	1871	181
1103–04A	106.9	– 4.33	2.16	– 13.31	– 13.19	– 23.7	– 4.57	– 23.8	– 4.70	4475	3604	2237	2321	1744	1802	1870	68
0127–11A	107.8	– 5.15	2.13	– 14.13	– 14.00	– 23.7	– 4.57	– 23.9	– 4.73	3456	2863	1728	1799	1380	1431	1501	70
0127–12A	108.8	– 6.14	1.71	– 15.12	– 14.99	– 23.6	– 4.48	– 24.3	– 5.11	2427	2056	1213	1272	983	1028	1269	241
1102–03bA	110.3	– 5.89	1.80	– 14.87	– 14.74	– 23.5	– 4.39	– 24.2	– 5.03	2589	2158	1294	1355	1034	1079	1331	252
0127–08A	111.1	– 4.31	1.84	– 13.29	– 13.17	– 23.5	– 4.39	– 24.2	– 4.99	4354	3435	2177	2260	1661	1717	2046	329
0127–07A	111.5	– 3.47	2.00	– 12.45	– 12.34	– 23.5	– 4.39	– 24.0	– 4.85	5675	4318	2838	2939	2095	2159	2458	298
NX-03	111.8	– 3.9	1.78	– 12.83	– 12.72	– 23.5	– 4.39	– 24.2	– 5.05	5033	3895	2516	2608	1888	1948	2350	402
YK-K1c-07	112.3	– 4.16	1.57	– 13.14	– 13.02	– 23.5	– 4.39	– 24.4	– 5.24	4570	3583	2285	2371	1734	1791	2286	495
0127–09A	112.7	– 5.41	1.25	– 14.39	– 14.26	– 23.5	– 4.39	– 24.8	– 5.53	3050	2503	1525	1592	1203	1252	1774	522
1109–04A	113.8	– 4.55	2.47	– 13.53	– 13.41	– 23.5	– 4.39	– 23.5	– 4.42	4035	3212	2018	2096	1552	1606	1619	13
0127–06A	114.8	– 3.82	2.64	– 12.80	– 12.69	– 23.5	– 4.39	– 23.4	– 4.26	5082	3928	2541	2634	1904	1964	1893	– 71
0127–05A	114.9	– 3.93	2.75	– 12.91	– 12.80	– 23.5	– 4.39	– 23.3	– 4.16	4909	3813	2455	2545	1847	1906	1783	– 123
LZ2–18A	115.3	– 4.20	2.63	– 13.18	– 13.06	– 23.5	– 4.39	– 23.4	– 4.27	4509	3541	2254	2339	1713	1770	1709	– 61
LZ2–12A	116.1	– 3.78	2.32	– 12.76	– 12.65	– 23.5	– 4.39	– 23.7	– 4.55	5146	3971	2573	2667	1925	1986	2082	96
LZ2–06A	117.8	– 5.35	1.46	– 14.33	– 14.20	– 23.5	– 4.39	– 24.5	– 5.34	3112	2548	1556	1623	1226	1274	1705	430
1108–03A	123.3	– 5.29	3.60	– 14.27	– 14.14	– 23.7	– 4.57	– 22.4	– 3.39	3304	2749	1652	1721	1324	1374	920	– 455
1108–01A	123.6	– 6.22	3.20	– 15.20	– 15.06	– 23.8	– 4.66	– 22.8	– 3.75	2474	2134	1237	1296	1021	1067	759	– 308
1108–02A	123.7	– 7.11	1.41	– 16.09	– 15.95	– 23.8	– 4.66	– 24.6	– 5.38	1780	1577	890	942	747	788	1030	241
TJ-05A	123.8	– 6.12	1.72	– 15.10	– 14.97	– 23.8	– 4.66	– 24.3	– 5.10	2561	2203	1280	1340	1055	1102	1272	171
ZC-27aA	126.4	– 6.40	1.28	– 15.38	– 15.24	– 24.0	– 4.85	– 24.7	– 5.50	2436	2146	1218	1276	1027	1073	1331	258
ZC-27bA	126.6	– 4.23	2.23	– 13.21	– 13.09	– 24.0	– 4.85	– 23.8	– 4.64	4840	4009	2420	2508	1941	2005	1887	– 118
1104–01A	127.5	– 3.85	2.16	– 12.83	– 12.72	– 24.1	– 4.94	– 23.8	– 4.70	5510	4557	2755	2852	2209	2279	2130	– 149
ZC-29bA	129.8	– 6.65	1.45	– 15.63	– 15.49	– 24.2	– 5.03	– 24.6	– 5.35	2342	2110	1171	1228	1008	1055	1175	120

Table 2. Continued.

		Time horizon (see table footnotes 1–16)															
Sample	Age (Ma)	1 $\delta^{13}C_c$	2 $\delta^{13}C_{oc}$	3 $\delta^{13}C_s$	4 $\delta^{13}C_{sc}$	5 $\delta^{13}C_r$	6 $\delta^{13}C_{ac}$	7 $\delta^{13}C_{roc}$	8 $\delta^{13}C_{aoc}$	9 pCO_2	10 pCO_2	11 pCO_2	12 pCO_2	13 pCO_2	14 pCO_2	15 pCO_2	16 pCO_2
ZC-29A	130.2	− 6.24	1.58	− 15.22	− 15.08	− 24.2	− 5.03	− 24.4	− 5.23	2687	2397	1344	1404	1149	1199	1279	80
ZC-32A	130.8	− 6.99	1.46	− 15.97	− 15.83	− 24.2	− 5.03	− 24.5	− 5.34	2078	1888	1039	1093	899	944	1053	109
ZC-37A	131.3	− 4.12	1.44	− 13.10	− 12.98	− 24.2	− 5.03	− 24.6	− 5.35	5156	4351	2578	2670	2108	2175	2387	212
0128–03A	132.0	− 3.27	1.18	− 12.25	− 12.14	− 24.3	− 5.12	− 24.8	− 5.59	6745	5600	3373	3486	2719	2800	3202	401

1. Measured carbon isotope composition of pedogenic carbonate from SE China.
2. Carbon isotope composition of well-dated marine carbonate from SE France (northern Tethys). Refer to text and caption of Figure 5.
3. Carbon isotope composition of pedogenic carbonate calibrated by temperature-dependent fractionation factor –8.98 ‰ (Ekart *et al*. 1999): $\delta^{13}C_s = 8.98 + \delta^{13}C_c$.
4. Carbon isotope composition of pedogenic carbonate at 25 °C based on palaeomagnetic data and latitude–temperature correlations (Besse & Courtillot, 1988; Ekart *et al*. 1999) following the formula of Romanek, Grossman & Morse (1992): $\delta^{13}C_{sc} = (\delta^{13}C_c + 1000)/[(11.98 - 0.12 \times T)/1000 + 1] - 1000$.
5. Carbon isotope composition of soil-respired CO_2, read in Figure 6 from the highly smoothed average of Ekart *et al*. (1999), reflecting atmospheric $\delta^{13}CO_2$ linearly across pCO_2 levels.
6. Atmospheric carbon isotopes calibrated by pedogenic organic matter ($\delta^{13}C_{ac} = (\delta^{13}C_r + 18.67)/1.1$; Arens, Jahren & Amundson, 2000), in which $\delta^{13}C_r$ is derived from the highly smoothed average of Ekart *et al*. (1999).
7. Carbon isotope composition of soil-respired CO_2 calculated using a −26 ‰ fractionation between the carbon isotope composition of well-dated marine carbonate from SE France (northern Tethys) and soil organic matter (Ekart *et al*. 1999).
8. Atmospheric carbon isotopes calibrated from pedogenic organic matter ($\delta^{13}C_{ac} = (\delta^{13}C_r + 18.67)/1.1$; Arens, Jahren & Amundson, 2000), in which $\delta^{13}C_r$ is derived from the measured carbon isotope composition of marine carbonate from SE France (northern Tethys).
9. Atmospheric pCO_2 estimated from the equation of Cerling (1999), using $S(z) = 5000$; $\delta^{13}C_s = \delta^{13}C_s$; $\delta^{13}C_ø = \delta^{13}C_r$; $\delta^{13}C_a = \delta^{13}C_a$
10. Atmospheric pCO_2 estimated from the equation of Cerling (1999), using $S(z) = 5000$; $\delta^{13}C_s = \delta^{13}C_{sc}$; $\delta^{13}C_r = \delta^{13}C_r$; $\delta^{13}C_a = \delta^{13}C_{ac}$
11. Atmospheric pCO_2 estimated from the equation of Cerling (1999), using $S(z) = 2500$; $\delta^{13}C_s = \delta^{13}C_s$; $\delta^{13}C_r = \delta^{13}C_r$; $\delta^{13}C_a = \delta^{13}C_a$
12. Atmospheric pCO_2 estimated from the equation of Cerling (1999), using $S(z) = 2500$; $\delta^{13}C_s = \delta^{13}C_s$; $\delta^{13}C_r = \delta^{13}C_r$; $\delta^{13}C_a = \delta^{13}C_a$
13. Atmospheric pCO_2 estimated from the equation of Cerling (1999), using $S(z) = 2500$; $\delta^{13}C_s = \delta^{13}C_{sc}$; $\delta^{13}C_r = \delta^{13}C_r$; $\delta^{13}C_a = \delta^{13}C_{ac}$
14. Atmospheric pCO_2 estimated from the equation of Cerling (1999), using $S(z) = 2500$; $\delta^{13}C_s = \delta^{13}C_s$; $\delta^{13}C_r = \delta^{13}C_r$; $\delta^{13}C_a = \delta^{13}C_{ac}$; of these, $\delta^{13}C_r$ is from the highly smoothed average of Ekart *et al*. (1999).
15. Atmospheric pCO_2 estimated from the formula of Cerling (1999), using $S(z) = 2500$; $\delta^{13}C_s = \delta^{13}C_{sc}$; $\delta^{13}C_r = \delta^{13}C_{roc}$; $\delta^{13}C_a = \delta^{13}C_{aoc}$; of these, $\delta^{13}C_r$ represents the −26 ‰ fractionation between oceanic carbonate and soil organic matter (Ekart *et al*. 1999) derived from the carbon isotope composition of shallow marine carbonate from SE France.
16. Discrepancy of atmospheric pCO_2 estimated by different $\delta^{13}C_r$ values as indicated in columns 14 and 15. pCO_2 in column 15 is on average 125 ppmV greater than that shown in column 14. The trend of pCO_2 changes is, however, similar in both columns 14 and 15.
Equation of pCO_2 is referred to in the text. $\delta^{13}C_a = -6.5$ ‰; $T = 25$ °C.

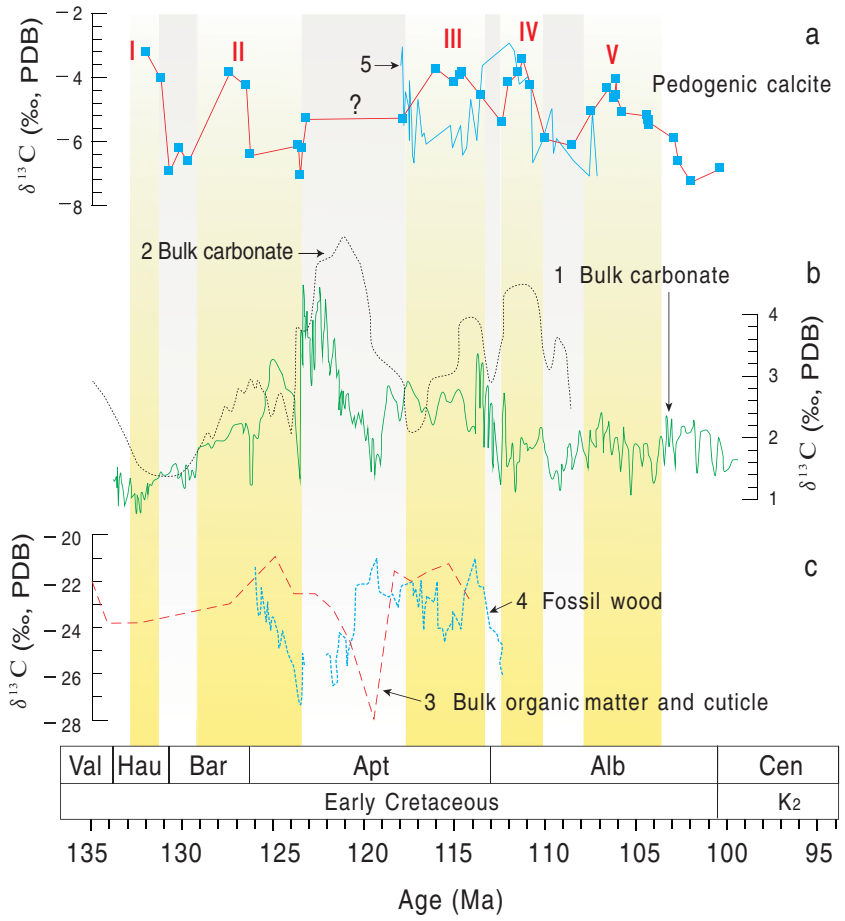

Figure 5. (Colour online) Correlation diagram of carbon isotope values from the Lower Cretaceous. Note that ages and stages are tuned to the time chart of Ogg, Hinnov & Huang (2012) using biostratigraphical correlation. (a) Pedogenic calcite, this work, shown as unfilled rectangles; (b) bulk carbonate; and (c) bulk organic matter (plant cuticle and fossil wood). (1) Five-point moving average from bulk marine hemipelagic carbonate from Northern Tethys (Col de Palluel, SE France), derived from Moullade *et al*. (1998), Hennig, Weissert & Bulot (1999), van de Schootbrugge *et al*. (2000), Herrle *et al*. (2004), Föllmi *et al.* (2006) and Gale *et al*. (2011). (2) Mainly pelagic bulk carbonate from other western Tethyan localities based on Weissert & Channell (1989), Channell, Erba & Lini (1993), Erba *et al.* (1999) and Herrle (2002). (3) Bulk organic matter and cuticle after Jahren *et al.* (2001): the lack of agreement between this and other curves is probably due to stratigraphic mis-assignment. (4) Fossil wood after Gröcke, Hesselbo & Jenkyns (1999). (5) Terrestrial calcrete after Ludvigson *et al.* (2010). Roman numerals and grey and yellow bands indicate cycles of repeated change in pedogenic carbon isotope values.

which are broadly consistent with those given by Ekart *et al*. (1999). Secondly, following the calibration of Arens, Jahren & Amundson (2000), the $\delta^{13}C_{aoc}$ (column 8 of Table 2) of atmospheric CO_2 values were calculated, also derived from carbon isotope values of pelagic sediment. Thirdly, C_a (pCO_2) was estimated using the formula of Cerling (1999). The resulting levels of pCO_2 are different from those derived from $\delta^{13}C_r$ of the highly smoothed average of Ekart *et al*. (1999) (cf. columns 14 and 15 of Table 2). The method utilizing $\delta^{13}C$ values of pelagic carbonate generally yielded higher values: 125 ppmV on average (column 16 of Table 2) and as much as 522 ppmV higher in one instance (but 455 ppmV lower in another instance). However, there is no distinct difference in the trend of the reconstructed pCO_2 between the two curves.

$S(z)$ is a function of depth but is effectively constant below 50 cm, where carbonates are precipitated (e.g. Cerling, 1991; Cerling & Quade, 1993). Both the (peaty organic matter) horizon O and (organic–clay) soil horizon A were not commonly preserved above the subsurface of concretion horizon Bk within the Cretaceous palaeosol, i.e. over 30–50 cm had been eroded. We generally undertook sampling in the middle of the horizon Bk (>30 cm Table S1, available at http://journals.cambridge.org/geo), which means that the depth of formation of the calcrete samples in the examined Cretaceous palaeosols was generally deeper than 50 cm below the palaeosol surface, meeting the requirement for a constant value of $S(z)$.

In earlier publications, a value of 5000 ppmV was often adopted for $S(z)$ in palaeoatmospheric CO_2 reconstructions. However, this value is much higher than those estimated by examination of plant stomata (e.g. Royer, 2006; Fletcher *et al.* 2008). Why this difference exists is not clear at present. Cerling (1991) gave values for $S(z)$ that were assumed to be 5 000–10 000 ppmV. Breecker, Sharp & McFadden (2010) interpreted the large discrepancy of $S(z)$ as due to large variations in atmospheric pCO_2 over relatively short time periods as

https://doi.org/10.1017/S0016756813000897 Published online by Cambridge University Press

well as inaccurate proxy estimates. They therefore used carbon isotope ratios of Holocene calcic soil to recalculate and calibrate atmospheric pCO_2 from a value of $S(z) = 2500$ ppmV, which agreed better with estimates from other proxies and the GEOCARB model. In this context, we also chose an $S(z)$ of 2500 ppmV for calculating pCO_2 at 25 °C (cf. Tables S2–4, available at http://journals.cambridge.org/geo), which compares more closely to estimates derived from plant cuticle. Clearly, however, the trend of pCO_2 over time is not altered by using different values of $S(z)$, and relative changes in atmospheric composition are still illustrated.

For comparison, the new data are illustrated together with previously published reconstructions for Cretaceous pCO_2 derived from both pedogenic calcite and stomatal indices of fossil plants (Figs 5, 6). The Cretaceous global composite curve of pCO_2 from pedogenic calcite comprises data from North America, England, India, South Korea, Japan and Tibet (Tables S3–S4, available at http://journals.cambridge.org/geo).

6. Results and discussion

6.a. Carbon isotope profiles

The carbon isotope profile shows that $\delta^{13}C$ values of calcites range from −3.0 ‰ to −7.0 ‰ (Figs 2, 5; Tables S2–S3, available at http://journals.cambridge.org/geo), as is typical for carbonate material of pedogenic origin (Fig. 4). Four complete and one incomplete increasing–decreasing stages of $\delta^{13}C$ values can be recognized: (I) early(?)–latest Hauterivian (*c.* 134–131 Ma); (II) earliest Barremian–early Aptian (*c.* 131–124 Ma); (III) early Aptian–earliest Albian (*c.* 124–113 Ma); (IV) earliest–middle Albian (*c.* 113–108 Ma); and (V) middle–late Albian (*c.* 108–102 Ma). Most stages have an estimated duration of *c.* 3.0–6 Ma.

Given the stratigraphic uncertainties, such patterns match global compilations in other materials in showing broad positive $\delta^{13}C$ excursions centred during late Barremian, latest Aptian and early Albian time (Fig. 5) and negative excursions during early Barremian, earliest Aptian and early and late Albian time: specifically, there is some level of agreement with isotopic records of bulk carbonate (Fig. 5b) from the Alpine Tethys and North Atlantic (e.g. Weissert, 1989; Erbacher, Thurow & Littke, 1996; Menegatti *et al.* 1998; Erba *et al.* 1999; Luciani, Cobianchi & Jenkyns, 2001; Herrle *et al.* 2004), the northern Tethys margin (Föllmi *et al.* 2006; Lorenzen *et al*. 2013) and the Middle East (Vahrenkamp, 2010), from a shallow-water Pacific guyot (Jenkyns & Wilson, 1999) and also with fossil wood ($\delta^{13}C_{org}$; Fig. 5c) from southern Britain (Gröcke, Hesselbo & Jenkyns, 1999; Robinson & Hesselbo, 2004). Abruptly decreasing $\delta^{13}C$ values at the boundary of the Barremian and Aptian stages, the early and middle Aptian and the earliest Albian stages can be observed in both Chinese pedogenic calcrete and French (northern Tethys) marine carbonates.

However, relatively high $\delta^{13}C$ values seen in the middle and late Aptian and low $\delta^{13}C$ values in the transition between the middle and late Aptian of bulk marine carbonate from western Tethys and in bulk organic and cuticle from South America (cf. Fig. 5a–c) are not seen in the Chinese pedogenic record, possibly due to sparse availability of calcrete in the critical intervals. The somewhat higher $\delta^{13}C$ values in pedogenic calcite from SE China during late Aptian and earliest Albian time conform to trends recognized in bulk carbonate from the Alpine Tethys, Atlantic and Pacific regions (Menegatti *et al.* 1998; Jenkyns & Wilson, 1999; Luciani, Cobianchi & Jenkyns, 2001; Herrle, 2002; Föllmi *et al.* 2006; Huber *et al.* 2011), bulk organic matter and plant cuticle from South America (Jahren *et al.* 2001) and fossil wood from southern England (e.g. Gröcke, Hesselbo & Jenkyns, 1999; Robinson & Hesselbo, 2004) and Japan (Ando *et al.* 2003). Overall, Albian $\delta^{13}C$ values decrease relatively smoothly, albeit punctuated by a positive excursion, in bulk marine organic matter, bulk pelagic carbonate and fossil wood (Erbacher, Thurow & Littke, 1996; Bralower *et al.* 1999; Luciani, Cobianchi & Jenkyns, 2004; Ando & Kakegawa, 2007), generally conforming to the pattern seen in the Chinese pedogenic calcrete.

Particularly noteworthy is the fact that absolute $\delta^{13}C$ values of pedogenic calcretes in SE China are similar to those of continental foreland-basin strata of the Cedar Mountain Formation in eastern Utah, USA (Ludvigson *et al.* 2010) and to those of the middle Aptian–Albian fluvial–lacustrine facies of the Liupanshan Group in NW China (Li *et al.* 2013) . Two stages of increasing–decreasing $\delta^{13}C$ values can also be recognized in the $\delta^{13}C$ sequence of the late Aptian–early Albian interval from Utah (*c.* 118–110 Ma), although there are some differences that could be caused by errors in age assignment in either or both sequences.

6.b. Estimations and comparisons of pCO_2

pCO_2 values from the Chinese calcretes mostly range between 1000 and 2500 ppmV (Figs 6–8), supporting the idea of both atmospheric CO_2 extremes and an accompanying greenhouse climate during mid-Cretaceous time based on $\delta^{18}O$ and Mg/Ca ratios in well-preserved planktonic foraminifera (Bice & Norris, 2002; Bice *et al.* 2006). The proposed pCO_2 levels are about 4–9 times the pre-industrial value of 275 ppmV and exceed this range during middle Hauterivian time (*c.* 132 Ma); an overall decrease in pCO_2 values from Hauterivian time to the end of Albian time, albeit with major fluctuations, can be observed (Figs 6–8).

The reconstructed pCO_2 is *c.* 20–50 % higher than the 600–1200 ppmV (recalculated using $S(z) = 2500$) of the global composite (Fig. 4a). It is notable that reconstructed pCO_2 from early–middle Albian time of SE China is 300–500 ppmV higher than that reconstructed from pedogenic calcretes in South Korea (Hong & Lee, 2012); during late Albian time, however, similar levels of 1000–1500 ppmV are reconstructed from

https://doi.org/10.1017/S0016756813000897 Published online by Cambridge University Press

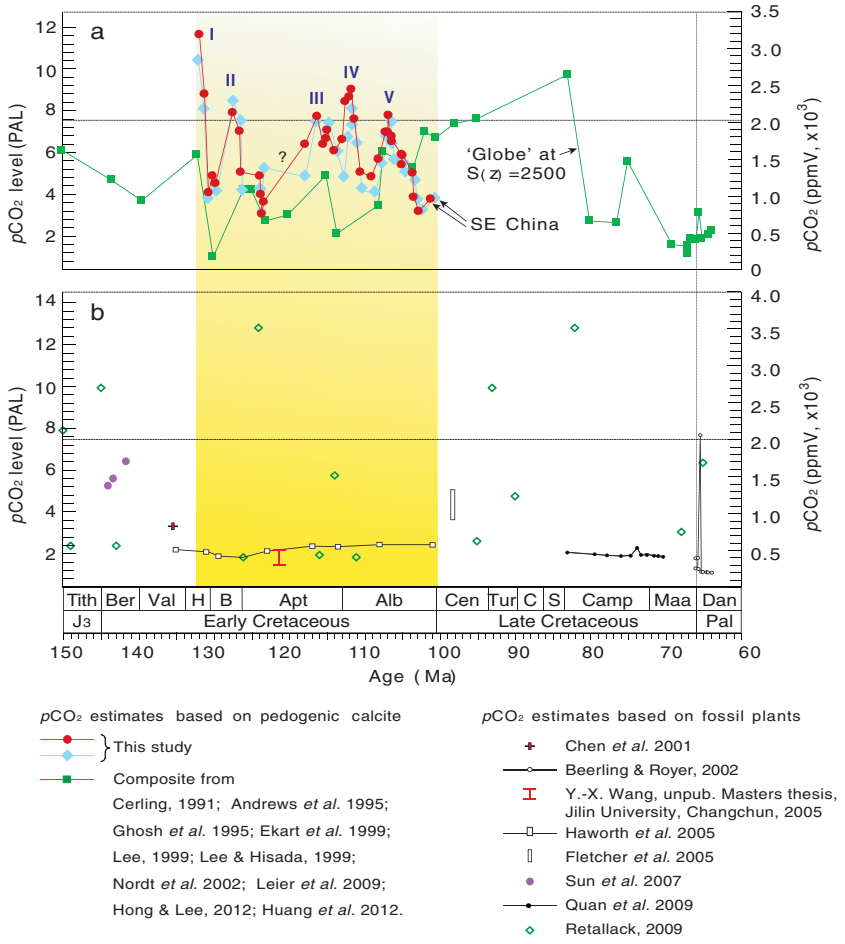

Figure 6. (Colour online) Comparison of the Cretaceous pCO_2 estimates determined from (a) carbon isotope proxies of pedogenic calcretes and (b) stomata. The global curve is sourced from the northern hemisphere continents using $S(z) = 2500$ ppmV. For all parameters used for estimating pCO_2 of the carbon isotopes of pedogenic calcite refer to Table 2 and Tables S3–S4 (available at http://journals.cambridge.org/geo) and for the fossil stomata refer to the references in the figure. All age data use the time scale of Ogg, Hinnov & Huang (2012) to be consistent with previous studies. Pre-industrial atmospheric pCO_2 level (PAL) is taken to be *c.* 275 ppmV. In (a), the curve of pCO_2 marked by blue diamonds is estimated from the highly smoothed average of $\delta^{13}C_r$ from Ekart *et al.* (1999), and the curve marked by red circles is obtained from isotopic data of Tethyan pelagic sediments. See also Andrews, Tandon & Dennis (1995), Ghosh, Bhattacharya & Jani (1995), Chen *et al.* (2001), Fletcher *et al.* (2005) and Y.-X. Wang, unpub. Masters thesis, Jilin University, Changchun (2005). Vertical yellow band indicates the time interval described in this study.

both regions. The cause of this discrepancy remains unknown, and may be partly attributed to large variations in atmospheric CO_2 over relatively short time periods and inaccurate proxy estimates (Breecker, Sharp & McFadden, 2010). However, the fractionation factor between CO_2 and precipitated calcite is dependent on temperature, global climate, palaeolatitude and palaeoelevation of formation of the different pedogenic calcites, and these factors may have played a role.

On the other hand, changes of pCO_2 reconstructed for SE China and the global composite show similar trends: the major falls during late Hauterivian, early Aptian and latest Aptian time and rises during early Hauterivian, late Aptian and middle Albian time are approximately coeval (Fig. 6a). Differences in the curves are observed for the global falls and Chinese rises during early Hauterivian and earliest Albian time, and for the global rise and Chinese fall during late Albian time (Fig. 6a). Discrepancies between the global and Chinese curves can be attributed to low stratigraphic sample resolution and inaccurate dating of specimens used in the global composite. Nevertheless, the general correlation supports the view that the Chinese pedogenic carbonate calcretes are appropriate for reconstruction of ancient pCO_2.

However, neither the pCO_2 reconstructions from SE China nor the global composite readily match the stomatal-index data from fossil plants (cf. Fig. 6a, b). The pCO_2 estimates of the Hauterivian–Albian interval based on stomata of the extinct conifer *Pseudofrenelopsis* in England and the United States (Haworth *et al.* 2005) are much lower than that reconstructed from the pedogenic calcite from SE China. Similar relative differences are seen when comparing Campanian pCO_2 estimates from fossil cuticle of *Ginkgo adiantoides* from NE China (Quan *et al.* 2009) with the pedogenic calcite from the global composite (Fig. 6a, b). The deviations between the stomatal and pedogenic calcrete pCO_2 values must indicate inappropriate application of one or more parameters in the production of either

https://doi.org/10.1017/S0016756813000897 Published online by Cambridge University Press

one or both proxies, as well as possible dating errors of both plant material and calcrete. Significantly, pCO_2 reconstructions from SE China have a similar general trend to those derived from $\delta^{13}C$ values of planktonic organic matter (Freeman & Hayes, 1992), i.e. pCO_2 was high during Early Cretaceous time (140–90 Ma) then fell thereafter. However, pCO_2 values reconstructed from pedogenic calcrete are almost double those derived from organic matter.

The mid-Cretaceous pCO_2 values determined from the Chinese deposits for some intervals are higher and for other intervals lower than those produced by modelling (Fig. 7; Berner, 1994, 2001, 2006; Tajika, 1999; Wallmann, 2001). Both the Chinese results and the data from GEOCARB III (Berner, 2001) and GEOCARBSULF (Berner, 2006) show a significant fall across the Hauterivian and Barremian stages (Fig. 5), indicating significant climate change over this interval. Secondly, a falling tendency during the late Aptian–Albian interval is observed after the increase of the early Aptian pCO_2 values in GEOCARB III (Berner, 2001) and GEOCARBSULF (Berner, 2006), as well as in the weathering index curve (Wallmann, 2001; Hansen & Wallmann, 2003) and the curve derived from magma eruption and organic carbon burial rate (Tajika, 1999). Thirdly, pCO_2 values in the Chinese pedogenic curve are relatively high during the late Aptian–middle Albian interval, albeit punctuated by two periods of relatively low values.

There are several major discrepancies between our data and the modelling results (Fig. 7). The initiation of the modelled fall in pCO_2 values started in Valanginian time and reached a minimum in Hauterivian (Tajika, 1999; Berner, 2001, 2006) or Barremian time (Wallmann, 2001; Hansen & Wallmann, 2003), earlier than indicated by the Chinese pedogenic studies (Fig. 7). Furthermore, at the time of the lowest modelled value in middle Barremian time (Tajika, 1999; Hansen & Wallmann, 2003), relatively high values are indicated by the data from China. This discrepancy could be attributed to relatively low resolution in the time increments examined in the generation of the models, such that distinct periodic changes in Aptian–Albian pCO_2 values reconstructed from pedogenically derived data are not captured (cf. Robinson *et al.* 2002). In addition, the secular decrease in pCO_2 reconstructed from Chinese pedogenic carbonates began in middle Albian time, *c.* 3–4 Ma earlier than those derived from modelling.

6.c. Explanations for rapid pCO_2 change

Regardless of the absolute values, a key point of our results is the rapid changes of pCO_2 registered during late Early Cretaceous time. Five rising–falling intervals are evident, similarly for changes in $\delta^{13}C$ values, namely during early(?)–middle Hauterivian time (*c.* 131 Ma), early Barremian–earliest Aptian time (*c.* 131–124 Ma) and earliest–latest Aptian time (*c.* 124–113 Ma). The absence of pedogenic data during early–middle Aptian time shows that intervals of rapid pCO_2 change may have been missed during earliest–middle Albian time (*c.* 113–108 Ma) and middle–late Albian time (*c.* 108–102 Ma); these intervals are numbered as events or periods I–V (Figs 6–8). Both the rapid rises and falls in pCO_2 occurred over intervals of *c.* 1–3 Ma, implying rapid changes in atmospheric composition and climatic fluctuations during this time rather than relatively high and largely invariant mid-Cretaceous pCO_2 conditions implied by many models (e.g. Berner, 2001, 2006; Wallmann, 2001; Hansen & Wallmann, 2003; Hong & Lee, 2012).

Substantial local sources of volcanogenic CO_2 over the interval in question could potentially include the late Mesozoic volcano-magmatic activity of the so-called late 'Yanshanian' sub-period in China (e.g. Ren & Chen, 1989; Zhang, 1998). In SE China, four periods of Cretaceous volcanism have been distinguished: 145–140 Ma, 130–125 Ma, 125–117 Ma and 117–105 Ma by K–Ar, Ar–Ar and Rb–Sr methods (Li, Shen & Wang, 1989). These latter three periods have been partly confirmed by zircon U–Pb dating (Wang *et al.* 2000; Fig. 2). Local volcanic eruption periods of 130–125 Ma and 117–105 Ma could correlate with the rising–falling stages II and III–V of pCO_2, respectively. The original volume of volcanic rocks and their degassing rate cannot be established, however, meaning that the relative importance of local volcanism in controlling pCO_2 is unknown. Furthermore, any cause-and-effect relationship between volcanism and pCO_2 remains uncertain in the absence of more precise dating.

As shown in Figures 6–8, our reconstructed model of rapid rises and falls in atmospheric pCO_2 during mid-Cretaceous time (five times within *c.* 30 Ma) seems consistent with the model of atmospheric CO_2 based on pedogenic calcretes (Schaller, Wright & Kent, 2011), linked to the formation of the Late Triassic–Early Jurassic central Atlantic magmatic province (CAMP), except in the magnitude of the inferred changes. The reconstruction of pre-CAMP atmospheric composition is of pCO_2 values of *c.* 2000 ppm that were subsequently increased to *c.* 4400 ppm ($S(z) = 3000 \pm 1000$ ppmV) immediately after the extrusion of the first volcanic unit that was presumably accompanied by effusion of volcanogenic CO_2. Subsequently, there was a steady decrease in pCO_2 towards pre-eruptive levels over the subsequent 0.3 Ma, interpreted as due to the effect of silicate weathering.

During the greenhouse Cretaceous Period a number of large igneous provinces (LIPs) were formed. Major volcanic pulses of Early Cretaceous LIPs took place around the interval 134–129 Ma (LIP1, Paraná and Etendeka traps and Comei-Bunbury LIP, onset 134 Ma, Janasi, Freitas & Heaman, 2011; mean 132 Ma, Zhu *et al.* 2009), 126–122 Ma (LIP2, Ontong Java Plateau, Manihiki Plateau and Hikurangi Plateau, end of Barremian time through early Aptian time; Kuroda *et al.* 2011) and 120–116 Ma (LIP3, Kerguelen Plateau–Rajmahal traps, mean *c.* 118 Ma; Wignall, 2001; Courtillot & Renne, 2003). If we ignore the

https://doi.org/10.1017/S0016756813000897 Published online by Cambridge University Press

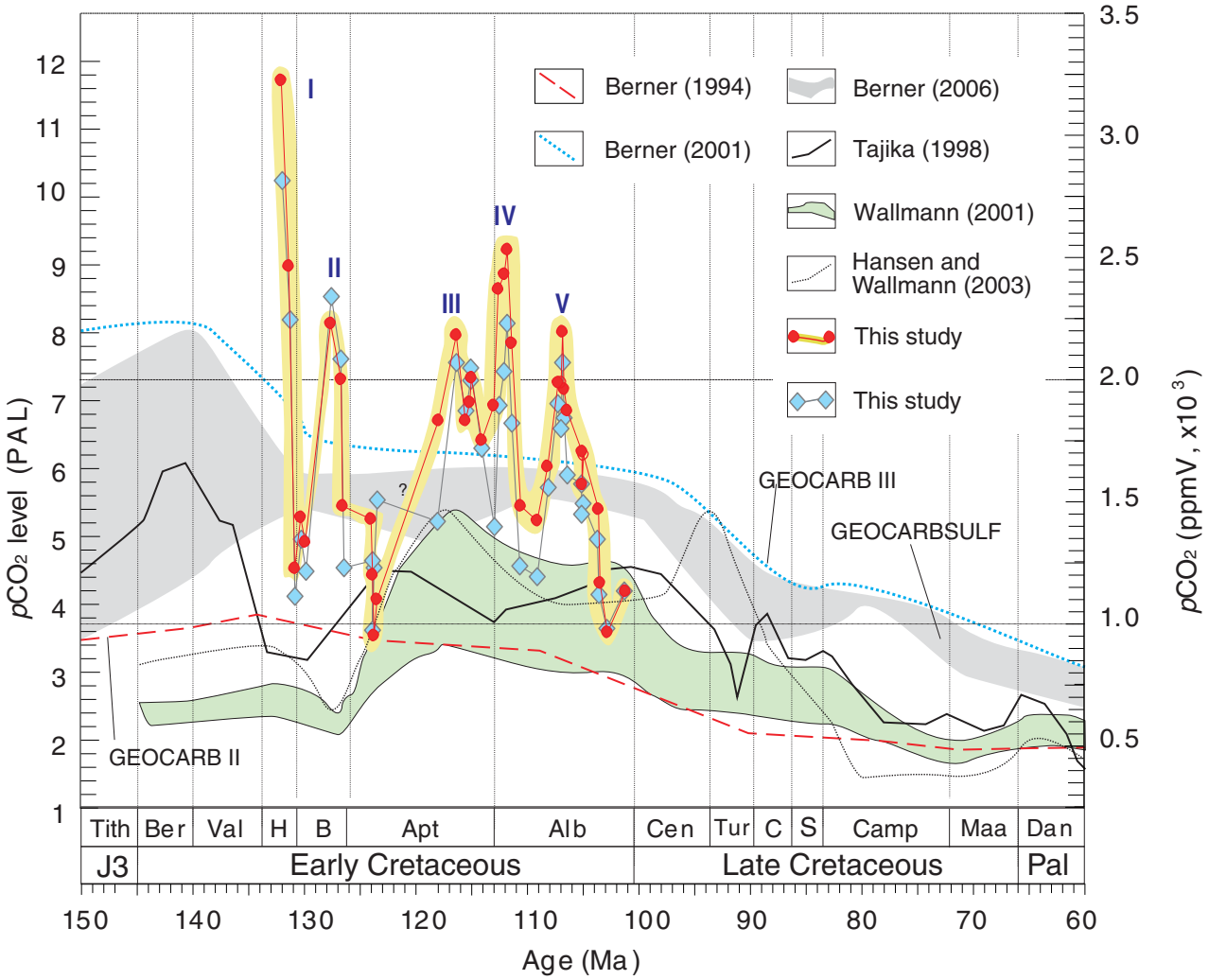

Figure 7. (Colour online) pCO_2 relationships between Cretaceous models and pedogenic estimates. The model curve of Tajika (1999) takes into account magma eruption and organic carbon burial rates; the Berner (1994) model is GEOCARB II; the Berner (2001) model is GEOCARB III; the Berner (2006) model is GEOCARBSULF; the Wallmann (2001) and Hansen & Wallmann (2003) curves model the global carbon–calcium–strontium cycle of seawater and atmosphere and silicate weatherability. Blue diamonds and red circles are as in Figure 6.

possible errors in dating of these volcanic edifices it is apparent that the intervals of rapid pCO_2 rise do not correspond in timing to the formation of Early Cretaceous LIPs (Fig. 8), whose extrusion would have been accompanied by large volumes of CO_2 (e.g. Arthur, Dean & Schlanger, 1985; Coffin & Eldholm, 1993; Larson & Erba, 1999). However, the extrusion periods of LIP1, LIP2 and LIP3 overlap with intervals of relatively rapid change in atmospheric pCO_2 as reconstructed from the Chinese record (Fig. 8). For example, reconstructed pCO_2 is particularly high during middle Hauterivian time and then falls to a relative minimum at the end of the stage, during which time extrusion of LIP1 apparently continued. The overall age of LIP eruptions is also incompatible with reconstructed Albian rising pCO_2 from the pedogenic record of South Korea (Hong & Lee, 2012). It is possible that the release of sediment-derived gases had a far greater impact on the environment than the emission of magmatic gases (Ganino & Arndt, 2009). It is therefore reasonable to believe that factors such as weathering rate, oceanic anoxic events (OAEs, carbon burial and CO_2 drawdown), degassing of magmatic bodies and dissociation of gas hydrates could have combined to generate a rapid change of pCO_2; volcanism was but one factor behind the elevation of pCO_2 values during the Early Cretaceous greenhouse period.

The Early–Middle Cretaceous Period was characterized by both major OAEs and more parochial environmental perturbations (Fig. 8), evidenced by relatively elevated depositional rates of marine organic matter and disturbances in the carbon isotope record that can manifest themselves as either positive or negative excursions. At its simplest, positive excursions should indicate burial of large amounts of organic matter and CO_2 drawdown; negative excursions should indicate injection of isotopically light carbon into the ocean–atmosphere system by addition of CH_4/CO_2. Such phenomena, commonly linked stratigraphically, are recorded from the late Valanginian (Weissert Event), latest

https://doi.org/10.1017/S0016756813000897 Published online by Cambridge University Press

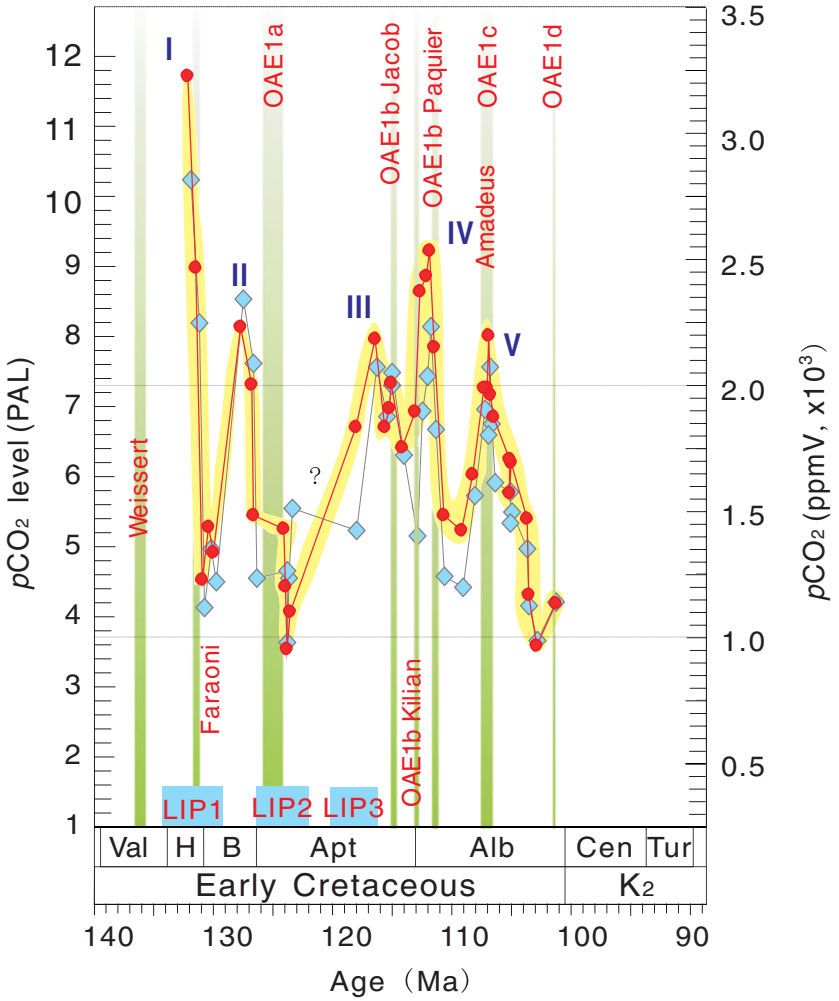

Figure 8. (Colour online) Ages of Cretaceous large igneous provinces (LIPs) and oceanic anoxic events (OAEs) in relation to the reconstructed Early Cretaceous pCO_2 in SE China (symbols as in Fig. 6). LIP 1: 134–129 Ma, Paraná and Etendeka traps (Janasi, Freitas & Heaman, 2011) and Comei-Bunbury LIP (Zhu *et al.* 2009); LIP 2: 126–122 Ma, Ontong Java Plateau, Manihiki Plateau and Hikurangi Plateau (summary by Kuroda *et al.* 2011); LIP 3: 120–116 Ma, Kerguelen Plateau–Rajmahal traps (Wignall, 2001; Courtillot & Renne, 2003). Weissert Event: 136.4–135.7 Ma, age data from Weissert & Lini (1991), Erba, Bartolini & Larson (2004), Ogg, Hinnov & Huang (2012); Faraoni Event, 131.3–131.1 Ma, from Bodin *et al.* (2006); OAE1a Selli/Goguel, 125.4–124.0 Ma, from summary of Ogg, Hinnov & Huang (2012); OAE1b Jacob, 115.1–114.9 Ma, from Herrle *et al.* (2004) and summary of Ogg, Hinnov & Huang (2012); OAE 1b Kilian Event, 113.3–113.0 Ma, from summary of Reboulet *et al.* (2011); OAE1b Paquier/Urbino, 111.3–111.1 Ma, from Gale *et al.* (2011) and summary of Ogg, Hinnov & Huang (2012); OAE1c Amadeus Segment, 107.2–106.7 Ma, from Leckie, Bralower & Cashman (2002) and summary of Ogg, Hinnov & Huang (2012); OAE1d Breistroffer, *c.* 101.1 Ma, from Erbacher, Thurow & Littke (1996), Leckie, Bralower & Cashman (2002) and summary of Ogg, Hinnov & Huang (2012). Blue diamonds and red circles are as in Figure 6.

Hauterivian (Faraoni Event), the early Aptian (OAE1a, Selli Event), the late Aptian (part of OAE1b, Jacob Event), the Aptian–Albian boundary (part of OAE 1b, Kilian Event), the early Albian (part of OAE1b, Paquier/Urbino Event), a possible middle Albian event (OAE1c, Jassines/Amadeus Event) and the late Albian (OAE1d, Breistroffer Event). They have been viewed as a response to 'ultrathermal' climatic conditions that forced increased silicate weathering, enhanced fluvial nutrient supply accompanied by vigorous upwelling and consequently increased plankton productivity and carbon flux to the seafloor, in some cases accompanied by introduction of isotopically light carbon from a crustal/sedimentary reservoir (Schlanger & Jenkyns, 1976; Arthur *et al.* 1990; Jenkyns, 2003, 2010; Herrle *et al.* 2004; Blättler *et al.* 2011; Gale *et al.* 2011; Reboulet *et al.* 2011; Bottini *et al.* 2012; Petrizzo *et al.* 2012). With OAEs, it is important to note that the run-up to the event itself generally correlates with rising global temperatures, but that the resulting widespread carbon burial and associated silicate weathering results in drawdown of CO_2 and an inverse greenhouse effect (Jenkyns, 2010). The prediction would therefore be for rising pCO_2 before such an event and falling pCO_2 after: distinct minima following pronounced maxima are potentially within range of both the Hauterivian Faraoni Event and the early Aptian OAE1a, given the uncertainties in the dating (Fig. 8).

Palaeotemperature data are necessarily regional: of note is evidence for early Barremian warming and

https://doi.org/10.1017/S0016756813000897 Published online by Cambridge University Press

late Barremian cooling from oxygen isotope values of north European belemnites (Podlaha, Mutterlose & Veizer, 1998; Malkoč & Mutterlose, 2010). These may be identifiable in the pedogenic pCO_2 record (Fig. 8), although these shifts cannot be readily disentangled from those of early Aptian shifts. A number of oxygen isotope studies of different parts of the world, together with palynological data from the Russian Platform and elsewhere, suggest globally increasing temperatures prior to the early Aptian OAE 1a followed by cooling (Menegatti *et al*. 1998; Hochuli *et al*. 1999; Price, 2003; Weissert & Erba, 2004; Ando *et al*. 2008; Zakharov *et al*. 2013); the movement of palaeotemperatures through the latter half of the Aptian appears, however, to be relatively modest. High-resolution indicators for drops in temperature of a few degrees during the early Aptian OAE1a itself derives from Pacific and Southern Ocean TEX_{86} records (Dumitrescu *et al.* 2006; Jenkyns *et al.* 2012) and from bulk-rock carbon and oxygen isotope data of a French marly subtropical intra-shelf basin (Kuhnt, Holbourn & Moullade, 2011) as well as from n-alkanes of biomarkers from the Cismon section, Italy (Méhay *et al.* 2009). However, only a modest drop in pCO_2 (based on comparative carbon isotope stratigraphy of algal biomarkers and bulk carbonate) was suggested for this interval by Heimhofer *et al.* (2004). The inferred drop in global temperature around the Aptian–Albian boundary (potentially defined by the Kilian Event), based on the high-latitude occurrence of glendonites, oxygen isotope data from Argentinian belemnites and cool-water biota (Kemper, 1987; Pirrie *et al.* 2004; Mutterlose, Bornemann & Herrle, 2009), supports the relatively low pCO_2 values reconstructed from the pedogenic record (Fig. 8). Available palaeotemperature data show a modest short-term rise during deposition of the Aptian–Albian boundary black shale, however (Kilian equivalent, in the Atlantic Ocean; Wagner *et al.* 2008; stratigraphy reassigned by Huber & Leckie, 2011; Petrizzo *et al.* 2012). Changes such as these are clearly not resolvable with the current pedogenic record. Relatively low $\delta^{13}C$ values for OAE1d during late Albian time were recorded from foraminiferal tests at ODP Site 1052, Blake Nose, western Atlantic (Wilson & Norris, 2001) and from both bulk organic matter and charcoals at Rose Creek Pit, Nebraska, Western Interior Basin, USA (Gröcke *et al.* 2006), correlating with low pCO_2 derived from Chinese pedogenic calcites.

A $\delta^{13}C_{org}$ curve recorded from fossil wood from Hokkaido, Japan well illustrates the negative excursion characteristic of OAE 1a. This is followed by a positive excursion, above which there is a generally falling trend interrupted by a positive excursion around the Aptian–Albian boundary with values irregularly declining higher in the section (Ando & Kakegawa, 2007). Such an isotopic profile shows a limited degree of compatibility with the pCO_2 trend derived from Chinese calcretes, again underscoring the complexities of the controls on levels of atmospheric carbon dioxide.

7. Summary and conclusions

The analysis of carbon isotopes from Lower Cretaceous pedogenic calcretes from SE China has yielded the following results and conclusions.

1. The $\delta^{13}C$ values of the pedogenic calcites range from –7.0 ‰ to –3.0 ‰. Four complete and one half (increasing–decreasing) excursions of $\delta^{13}C$ can be recognized: (I) early(?)–middle Hauterivian (*c.* 134–131 Ma); (II) early Barremian–earliest Aptian (*c.* 130–124 Ma); (III) earliest–latest Aptian (*c.* 124–113 Ma); (IV) earliest–middle Albian (*c.* 113–108 Ma); and (V) middle–late Albian (*c.* 108–102 Ma). During Barremian and late Aptian–earliest Albian time, the higher $\delta^{13}C$ values in pedogenic calcite from SE China conform to trends recognized in bulk carbonate from the Alpine Tethys, bulk organic matter and plant cuticle from South America and fossil wood from southern England and Japan.

2. Reconstructed pCO_2 from pedogenic carbonates of Hauterivian–Albian age mostly range from 1000 to 2500 ppmV at $S(z) = 2500$ ppmV (4–9 times pre-industrial values), much higher than that reconstructed from coeval stomatal indices in fossil plants and 20–50 % higher than the 600–1200 ppmV of the global composite curve. These results are, however, more consistent with those produced by modelling.

3. Rapid rises in pCO_2 identified for the individual 2–3 Ma interval of early Hauterivian (*c.* 134–132 Ma), early Barremian (*c.* 130–127 Ma), middle Aptian (*c.* 124–121 Ma), earliest Albian (*c.* 113–111 Ma) and middle Albian (*c.* 109–107 Ma) time and succeeding rapid falls imply major rapid climatic fluctuations during this time.

4. The changes in pCO_2 cannot be attributed to local volcanism and do not coincide exactly with the development of LIPs, whose formation could have vented large volumes of carbon dioxide into the atmosphere.

5. There is no simple relationship between estimated pCO_2 and global carbon isotope curves. This demonstrates that carbon burial is not the only factor controlling the quantity of carbon dioxide in the atmosphere, and that silicate weathering could also have been responsible for drawdown of this greenhouse gas. Degassing from the extrusion of LIPs together with dissociation of gas hydrates may have induced transient high pCO_2 values. It is suggested that the combination of these various factors could have led to rapid and repeated changes of pCO_2 during Early Cretaceous time.

Acknowledgments. We are grateful to the reviewers for their helpful comments and constructive suggestions. Drs Sijing Liang and Sidun Chen are thanked for participating in the field work. We also thank National Natural Science Foundation of China (Climatic changes and atmospheric CO_2 concentration estimate of the Cretaceous–Palaeogene from South China: 41372106) and National Basic Research Program of China (973 Program) 2012CB822003 for supporting this work.

References

ALONSO-ZARZA, A. M. 2003. Palaeoenvironmental significance of palustrine carbonates and calcretes in the geological record. *Earth-Science Reviews* **60**, 261–98.

ANDERSEN, T. 2002. Correction of common lead in U–Pb analyses that do not report ^{204}Pb. *Chemical Geology* **192**, 59–79.

ANDO, A., KAIHO, K., KAWAHATA, H. & KAKEGAWA, K. 2008. Timing and magnitude of early Aptian extreme warming: Unraveling primary $\delta^{18}O$ variation in indurated pelagic carbonates at Deep Sea Drilling Project Site 463, central Pacific Ocean. *Palaeogeography, Palaeoclimatology, Palaeoecology* **260**, 463–76.

ANDO, A. & KAKEGAWA, T. 2007. Carbon isotope records of terrestrial organic matter and occurrence of planktonic foraminifera from the Albian stage of Hokkaido, Japan: ocean-atmosphere $\delta^{13}C$ trends and chronostratigraphic implications. *Palaios* **22**, 417–32.

ANDO, A., KAKEGAWA, T., TAKASHIMA, R. & SAITO, T. 2003. Stratigraphic carbon isotope fluctuations of detrital woody materials during the Aptian Stage in Hokkaido, Japan: comprehensive $\delta^{13}C$ data from four sections of the Ashibetsu area. *Journal of Asian Earth Sciences* **21**, 835–47.

ANDREWS, J. E., TANDON, S. K. & DENNIS, P. F. 1995. Concentration of carbon dioxide in the Late Cretaceous atmosphere. *Journal of the Geological Society, London* **152**, 1–3.

ARENS, N. C., JAHREN, A. H. & AMUNDSON, R. 2000. Can C3 plants faithfully record the carbon isotopic composition of atmospheric carbon dioxide? *Paleobiology* **26**, 137–64.

ARTHUR, M. A., BRUMSACK, H. J., JENKYNS, H. C. & SCHLANGER, S. O. 1990. Stratigraphy, geochemistry, and paleoceanography of organic carbon-rich Cretaceous sequence. In *Cretaceous Resource, Events, and Rhythms* (eds R. N. Ginsburg & B. Beaudoin), pp. 75–119. Dordrecht: Kluwer.

ARTHUR, M. A., DEAN, W. E. & SCHLANGER, S. O. 1985. Variations in the global carbon cycle during the Cretaceous related to climate, volcanism, and changes in atmospheric CO_2: natural variations Archean to Present. In *The Carbon Cycle and Atmospheric CO_2* (eds E. T. Sundquist and W. S. Broecker), pp. 504–29. Monograph American Geophysical Union **32**.

BEERLING, D. J. & BERNER, R. A. 2005. Feedbacks and the coevolution of plants and atmospheric CO_2. *Proceedings of the National Academy of Sciences* **102**, 1302–5.

BEERLING, D. J., MCELWAIN, J. C. & OSBORNE, C. P. 1998. Stomatal responses of the 'living fossil' *Ginkgo biloba* L. to changes in atmospheric CO_2 concentrations. *Journal of Experimental Botany* **49**, 1603–7.

BEERLING, D. J. & ROYER, D. L. 2002. Reading a CO_2 signal from fossil stomata. *The New Phytologist* **153**, 387–97.

BERNER, R. A. 1994. GEOCARB II: A revised model of atmospheric CO_2 over Phanerozoic time. *American Journal of Science* **294**, 56–91.

BERNER, R. A. 2001. Modelling atmospheric O_2 over Phanerozoic time. *Geochimica et Cosmochimica Acta* **65**, 685–94.

BERNER, R. A. 2006. Inclusion of the weathering of volcanic rocks in the GEOCARBSULF model. *American Journal of Science* **306**, 295–302.

BESSE, J. & COURTILLOT, V. 1988. Paleogeographic maps of the continents bordering the Indian Ocean since the Early Jurassic. *Journal of Geophysical Research* **93**, 11791–808.

BICE, K. L., BIRGEL, D., MEYERS, P. A., DAHL, K. A., HINRICHS, K.-U. & NORRIS, R. D. 2006. A multiple proxy and model study of Cretaceous upper ocean temperatures and atmospheric CO_2 concentrations. *Paleoceanography* **21**, PA2002, doi: 10.1029/2005PA001203.

BICE, K. L. & NORRIS, R. D. 2002. Possible atmospheric CO_2 extremes of the Middle Cretaceous (late Albian–Turonian). *Paleoceanography* **17**, 1070, doi: 10.1029/2002PA000778.

BLACK, L. P. & GULSON, B. L. 1978. The age of the Mud Tank carbonatite, Strangways Range, Northern Territory. *Bureau of Mineral Resources Journal of Australian Geology and Geophysics* **3**, 227–32.

BLÄTTLER, C. L., JENKYNS, H. C., REYNARD, L. M. & HENDERSON, G. M. 2011. Significant increases in global weathering during Oceanic Anoxic Events 1a and 2 indicated by calcium isotopes. *Earth and Planetary Science Letters* **309**, 77–88.

BODIN, S., GODET, A., FÖLLMI, K. B., VERMEULEN, J., ARNAUD, H., STRASSER, A., FIET, N. & ADATTE, T. 2006. The late Hauterivian Faraoni oceanic anoxic event in the western Tethys: evidence from phosphorus burial rates. *Palaeogeography, Palaeoclimatology, Palaeoecology* **235**, 245–64.

BOTTINI, C., COHEN, A. S., ERBA, E., JENKYNS, H. C. & COE, A. L. 2012. Osmium-isotope evidence for volcanism, weathering, and ocean mixing during the early Aptian OAE 1a. *Geology* **40**, 583–6.

BRALOWER, T. J., COBABE, E., CLEMENT, B., SLITER, W. V., OSBURN, C. L. & LONGORIA, J. 1999. The record of global change in mid-Cretaceous (Barremian–Albian) sections from the Sierra Madre, northeastern Mexico. *Journal of Foraminiferal Research* **29**, 418–37.

BREECKER, D. O., SHARP, Z. D. & MCFADDEN, L. D. 2010. Atmospheric CO_2 concentrations during ancient greenhouse climates were similar to those predicted for A.D. 2100. *Proceedings of the National Academy of Sciences* **107**, 576–80.

BUCHMANN, N., BROOKS, R. J., FLANAGAN, L. B. & EHLERINGER, J. R. 1998. Carbon isotope discrimination of terrestrial ecosystems. In *Stable Isotopes: Integration of Biological, Ecological and Geochemical Processes* (ed. H. Griffiths), pp. 203–21. Oxford, Unitied Kingdom: BIOS Scientific Publications.

CAO, M. 1986 Lower Cretaceous ostracods from the Hekow Formation, Fujian. *Acta Palaeontologica Sinica* **25**, 239–47 (in Chinese with English abstract).

CERLING, T. E. 1991. Carbon dioxide in the atmosphere: evidence from Cenozoic and Mesozoic paleosols. *American Journal of Science* **291**, 377–400.

CERLING, T. E. 1999. Stable carbon isotopes in palaeosol carbonates. In *Palaeoweathering, Palaeosurfaces and Related Continental Deposits* (eds M. Thiry & R. Simon-Coinçon), pp. 43–60. Special Publication of the International Association of Sedimentologists 27.

CERLING, T. E. & QUADE, J. 1993. Stable carbon and oxygen isotopes in soil carbonates. In *Climate Change in Continental Isotopic Records* (eds P. K. Swart, K. C. Lohmann, J. A. McKenzie & S. Savin), pp. 217–31. Washington DC: American Geophysical Union.

CHANNELL, J. E. T., ERBA, E. & LINI, A. 1993. Magnetostratigraphic calibration of the late Valanginian carbon isotope event in pelagic limestones from northern Italy and Switzerland. *Earth and Planetary Science Letters* **118**, 145–66.

CHEN, C., LEE, C., LU, H. & HSEH, P. 2008. Generation of Late Cretaceous silicic rocks in SE China: age, major

element and numerical simulation constraints. *Journal of Asian Earth Sciences* **31**, 479–98.

CHEN, J.-H., KOMATSU, T., CAO, M.-Z. & STILLER, F. 2006. *Kumamotoa*, an early Late Cretaceous non-marine bivalve, from Fujian, south China. *Journal of Asian Earth Sciences* **27**, 943–51.

CHEN, L.-Q., LI, C.-S., CHALONER, W. G., BEERLING, D. J., SUN, Q.-G., COLLINSON, M. E. & MITCHELL, P. L. 2001. Assessing the potential for the stomatal characters of extant and fossil *Ginkgo* leaves to signal atmospheric CO_2 change. *American Journal of Botany* **88**, 1309–15.

CHEN, W., CHEN, P., XU, X. & ZHANG, M. 2005. Geochemical characteristics of Cretaceous basaltic rocks in South China and constraints on Pacific Plate subduction. *Science in China (Series D, Earth Sciences)* **48**, 2104–17.

COFFIN, M. F. & ELDHOLM, O. 1993. Scratching the surface: estimating dimensions of Large Igneous Provinces. *Geology* **21**, 515–8.

COURTILLOT, V. E. & RENNE, P. R. 2003. On the ages of flood basalt events. *Comptes Rendus Geoscience* **335**, 113–40.

DUMITRESCU, M., BRASSELL, S. C., SCHOUTEN, S., HOPMANS, E. C. & SINNINGHE DAMSTÉ, J. S. 2006. Instability in tropical Pacific sea-surface temperatures during the early Aptian. *Geology* **34**, 833–6.

EKART, D. D., CERLING, T. E., MONTAÑEZ, I. P. & TABOR, N. J. 1999. A 400 million year carbon isotope record of pedogenic carbonate: implications for paleoatmospheric carbon dioxide. *American Journal of Science* **299**, 805–27.

ERBA, E., BARTOLINI, A. & LARSON, R. L. 2004. Valanginian Weissert oceanic anoxic event. *Geology* **32**, 149–52.

ERBA, E., CHANNELL, J. E. T., CLAPS, M., JONES, C., LARSON, R., OPDYKE, B., PREMOLI SILVA, I., RIVA, A., SALVINI, G. & TORRICELLI, S. 1999. Integrated stratigraphy of the Cismon Apticore (Southern Alps, Italy): A 'reference section' for the Barremian–Aptian interval at low latitudes. *Journal of Foraminiferal Research* **29**, 371–92.

ERBACHER, J., THUROW, J. & LITTKE, R. 1996. Evolution patterns of radiolaria and organic matter variations: a new approach to identify sea-level changes in mid-Cretaceous pelagic environments. *Geology* **24**, 499–502.

FLETCHER, B. J., BEERLING, D. J., BRENTNALL, S. J. & ROYER, D. L. 2005. Fossil bryophytes as recorders of ancient CO_2 levels: experimental evidence and a Cretaceous case study. *Global Biogeochemical Cycles* **19**, 1–13.

FLETCHER, B. J., BRENTNALL, S. J., ANDERSON, C. W., BERNER, R. A. & BEERLING, D. J. 2008. Atmospheric carbon dioxide linked with Mesozoic and early Cenozoic climate change. *Nature Geoscience* **1**, 43–7.

FÖLLMI, K. B., GODET, A., BODIN, S. & LINDER, P. 2006. Interactions between environmental change and shallow water carbonate buildup along the northern Tethyan margin and their impact on the Early Cretaceous carbon isotope record. *Paleoceanography* **21**, PA4211, doi:10.1029/2006PA001313.

FRANÇOIS, L., GRARD, A. & GODDÉRIS, Y. 2005. Modelling atmospheric CO_2 changes at geological time scales. In *Pre-Cambrian to Palaeozoic Palaeopalynology and Palaeobotany* (eds P. Steemans & E. Javaux). Carnets de Géologie (Notebooks on Geology), Brest, Memoir **2**, Abstract 02 (CG2005-M02/02).

FREEMAN, K. H. & HAYES, J. M. 1992. Fractionation of carbon isotopes by phytoplankton and estimates of ancient CO_2 levels. *Global Biogeochemical Cycles* **6**, 185–98.

GALE, A. S., BOWN, P., CARON, M., CRAMPTON, J., CROWHURST, S. J., KENNEDY, W. J., PETRIZZO, M. R. & WRAY, D. S. 2011. The uppermost Middle and Upper Albian succession at the Col de Palluel, Hautes-Alpes, France: an integrated study (ammonites, inoceramid bivalves, planktonic foraminifera, nannofossils, geochemistry, stable oxygen and carbon isotopes, cyclostratigraphy). *Cretaceous Research* **32**, 59–130.

GANINO, C. & ARNDT, N. T. 2009. Climate changes caused by degassing of sediments during the emplacement of large igneous provinces. *Geology* **37**, 323–6.

GHOSH, P., BHATTACHARYA, S. K. & JANI, R. A. 1995. Paleoclimate and paleovegetation in central India during the Upper Cretaceous based on stable isotope composition of the paleosol carbonate. *Palaeogeography, Palaeoclimatology, Palaeoecology* **114**, 285–96.

GRÖCKE, D. R., HESSELBO, S. P. & JENKYNS, H. C. 1999. Carbon-isotope composition of Lower Cretaceous fossil wood: ocean-atmosphere chemistry and relation to sea-level change. *Geology* **27**, 155–8.

GRÖCKE, D. R., LUDVIGSON, G. A., WITZKE, B. L., ROBINSON, S. A., JOECKEL, R. M., UFNAR, D. F. & RAVN ROBERT, L. A. 2006. Recognizing the Albian–Cenomanian (OAE1d) sequence boundary using plant carbon isotopes: Dakota Formation, Western Interior Basin, USA. *Geology* **34**, 193–6.

HANSEN, K. W. & WALLMANN, K. 2003. Cretaceous and Cenozoic evolution of seawater composition, atmospheric O_2 and CO_2: a model perspective. *American Journal of Science* **303**, 94–148.

HAWORTH, H., HESSELBO, S. P., MCELWAIN, J. C., ROBINSON, S. A. & BRUNT, J. W. 2005. Mid-Cretaceous pCO_2 based on stomata of the extinct conifer *Pseudofrenelopsis* (Cheirolepidiaceae). *Geology* **33**, 749–52.

HEIMHOFER, U., HOCHULI, P. A., HERRLE, J. O., ANDERSEN, N. & WEISSERT, H. 2004. Absence of major vegetation and palaeoatmospheric pCO_2 changes associated with oceanic anoxic event 1a (Early Aptian, SE France). *Earth and Planetary Science Letters* **223**, 303–18.

HENNIG, S., WEISSERT, H. & BULOT, L. 1999. C-isotope stratigraphy, a calibration tool between ammonite- and magnetostratigraphy: the Valanginian-Hauterivian transition. *Geologica Carpatica* **50**, 91–6.

HERRLE, J. O. 2002. Paleoceanographic and paleoclimatic implications on mid-Cretaceous black shale formation in the Vocontian Basin and the Atlantic: evidence from calcareous nannofossils and stable isotopes. *Tübinger Mikropaldontologische Mitteilungen* **27**, 1–114.

HERRLE, J. O., KÖßLER, P., FRIEDRICH, O., ERLENKEUSER, H. & HEMLEBEN, C. 2004. High-resolution carbon isotope records of the Aptian to Lower Albian from SE France and the Mazagan Plateau (DSDP Site 545): a stratigraphic tool for paleoceanographic and paleobiologic reconstruction. *Earth and Planetary Science Letters* **218**, 149–61.

HOCHULI, P. A., MENEGATTI, A. P., WEISSERT, H., RIVA, A., ERBA, E. & PREMOLI SILVA, I. 1999. Episodes of high productivity in the early Aptian Alpine Tethys. *Geology* **27**, 657–60.

HONG, S. K. & LEE, Y. IL. 2012. Evaluation of atmospheric carbon dioxide concentrations during the Cretaceous. *Earth and Planetary Science Letters* **327–8**, 23–8.

HU, H., HU, S., WANG, S. & ZHU, M. 1982. Jurassic and Cretaceous age of volcanic rocks on isotope dating. *Acta Geologica Sinica* **56**, 315–22 (in Chinese with English abstract).

HU, L., LI, P. & MA, X. 1990. A magnetostratigraphic study of Cretaceous red beds from Shang-Hang, western Fujian. *Geology of Fujian* **9**, 33–42 (in Chinese).

HUANG, C. M., RETALLACK, G. J. & WANG, C. S. 2012. Early Cretaceous atmospheric pCO_2 levels recorded from pedogenic carbonates in China. *Cretaceous Research* **33**, 42–9.

HUBER, B. T. & LECKIE, R. M. 2011. Planktic foraminiferal species turnover across deep-sea Aptian/Albian boundary sections. *Journal of Foraminiferal Research* **41**, 53–95.

HUBER, B. T., MACLEOD, K. G., GRÖCKE, D. R. & KUCERA, M. 2011. Paleotemperature and paleosalinity inferences and chemostratigraphy across the Aptian/Albian boundary in the subtropical North Atlantic. *Paleoceanography* **26**, PA4211, doi: 10.1029/2001PA002178.

JACKSON, S. E., PEARSON, N. J., GRIFFIN, W. L. & BELOUSOVA, E. A. 2004. The application of laser ablation–inductively coupled plasma–mass spectrometry to in situ U/Pb zircon geochronology. *Chemical Geology* **211**, 47–69.

JAHREN, A. H., ARENS, N. C. & HARBESON, S. A. 2008. Prediction of atmospheric $\delta^{13}CO_2$ using fossil plant tissues. *Reviews of Geophysics* **46**, RG1002, doi: 10.1029/2006RG000219.

JAHREN, A. H., ARENS, N. C., SARMIENTO, G., GUERRERO, J. & AMUNDSON, R. 2001. Terrestrial record of methane hydrate dissociation in the Early Cretaceous. *Geology* **29**, 159–62.

JANASI, V. A., FREITAS, V. A. & HEAMAN, L. H. 2011. The onset of flood basalt volcanism, Northern Paraná Basin, Brazil: a precise U–Pb baddeleyite/zircon age for a Chapecó-type dacite. *Earth and Planetary Science Letters* **302**, 147–53.

JENKYNS, H. C. 2003. Evidence for rapid climate change in the Mesozoic–Palaeogene greenhouse world. *Philosophical Transactions of the Royal Society of London, Series A* **361**, 1885–916.

JENKYNS, H. C. 2010. Geochemistry of oceanic anoxic events. *Geochemistry, Geophysics, Geosystems* **11**, Q03004, doi: 10.1029/2009GC002788.

JENKYNS, H. C., SCHOUTEN-HUIBERS, L., SCHOUTEN, S. & SINNINGHE-DAMSTÉ, J. S. 2012. Warm Middle Jurassic–Early Cretaceous high-latitude sea-surface temperatures from the Southern Ocean. *Climates of the Past* **8**, 215–26.

JENKYNS, H. C. & WILSON, P. A. 1999. Stratigraphy, paleoceanography, and evolution of Cretaceous Pacific guyots: relics from a greenhouse Earth. *American Journal of Science* **299**, 341–92.

KEMPER, E. 1987. Das Klima der Kreide-Zeit. *Geologisches Jahrbuch Reihe A* **96**, 5–185.

KUHNT, W., HOLBOURN, A. & MOULLADE, M. 2011. Transient global cooling at the onset of early Aptian oceanic anoxic event (OAE)1a. *Geology* **39**, 323–6.

KURODA, J., TANIMIZU, M., HORI, R. S., SUZUKI, K., OGAWA, N. O., TEJADA, M. L. G., COFFIN, M. F., COCCIONI, R., ERBA, E. & OHKOUCHI, N. 2011. Lead isotopic record of Barremian-Aptian marine sediments: Implications for large igneous provinces and the Aptian climatic crisis. *Earth and Planetary Science Letters* **307**, 126–34.

LARSON, R. L. & ERBA, E. 1999. Onset of the Mid-Cretaceous greenhouse in the Barremian– Aptian: Igneous events and the biological, sedimentary, and geochemical responses. *Paleoceanography* **14**, 663–78.

LECKIE, R. M., BRALOWER, T. J. & CASHMAN, R. 2002. Oceanic anoxic events and plankton evolution: biotic response to tectonic forcing during the mid-Cretaceous. *Paleoceanography* **17**, 1041, doi: 10.1029/2001PA000623.

LEE, Y. I. 1999. Stable isotopic composition of calcic paleosols of the Early Cretaceous Hasandong Formation, southeastern Korea. *Palaeogeography, Palaeoclimatology, Palaeoecology* **150**, 123–33.

LEE, Y. I. & HISADA, K. 1999. Stable isotopic composition of pedogenic carbonates of the Early Cretaceous Shimonoseki Subgroup, western Honshu, Japan. *Palaeogeography, Palaeoclimatology, Palaeoecology* **153**, 127–38.

LEIER, A. L., QUADE, J., DECELLES, P. & KAPP, P. 2009. Stable isotopic results from paleosol carbonate in South Asia. Paleoenvironmental reconstructions and selective alteration. *Earth and Planetary Science Letters* **279**, 242–54.

LI, K.-Y., SHEN, J. & WANG, X. 1987. The source and evolution of parent magma of Mesozoic volcanics in Zhejiang, Fujian and Jiangxi. *Bulletin of the Nanjing Institute of Geology and Mineral Resources, Chinese Academy of Geological Sciences* **8**, 15–25 (in Chinese with English abstract).

LI, K.-Y., SHEN, J. & WANG, X. 1989. Isotopic geochronology of Mesozoic terrestrial volcanic rocks in Zhejiang, Fujian and Jiangxi China. *Journal of Stratigraphy* **13**, 1–13 (in Chinese with English abstract).

LI, X., CHEN, S., CAO, K., CHEN, Y., XU, B. & JI, Y. 2009. Paleosols of the mid-Cretaceous: a report from Zhejiang and Fujian, SE China. *Earth Science Frontiers* **16**, 63–70.

LI, X., CHEN, S., LUO, J., WAN, Y., CAO, K. & LIU, L. 2011. Single zircon U–Pb isotope chronology of the Early Cretaceous Jiande Group from western Zhejiang, SE China: Significances to stratigraphy. *Geological Review* **57**, 825–36 (in Chinese with English abstract).

LI, X., XU, W., LIU, W., ZHOU, Y., WANG, Y., SUN, Y., LIU, L. 2013. Climatic and environmental indications of carbon and oxygen isotopes from the Lower Cretaceous calcrete and lacustrine carbonates in Southeast and Northwest China. *Palaeogeography, Palaeoclimatology, Palaeoecology* **385**, 171–89.

LIU, C., ZHU, R.-X., JIN, Z.-X., LU, L.-Z. & DU, Y.-H. 1992. The study on magnetostratigraphy of Cretaceous in Laozhu District of Lishui, Zhejiang, China. In *Advances in Geoscience* (ed. S. Wang), pp. 104–10. China Ocean Press, Beijing, China (in Chinese with English abstract).

LIU, F.-Y., WU, J.-H. & LIU, S. 2009. Early Cretaceous zircon SHRIMP U-Pb age of the trachyte and its significances of the Gan-Hang Belt. *Journal of East China Institute of Technology* **32**, 330–5 (in Chinese with English abstract).

LIU, X. 1982. Recognition of the Yanshanian movement in the eastern part of China. *Geological Review* **5**, 1–4 (in Chinese with English abstract).

LORENZEN, J., KUHNT, W., HOLBOURN, A., FLÖGEL, S., MOULLADE, M. & TRONCHETTI, G. 2013. A new sediment core from the Bedoulian (Lower Aptian) stratotype at Roquefort-La Bédoule, SE France. *Cretaceous Research* **39**, 6–16.

LU, Q., ZHU, G. & QIN, Z. 2000. The characteristics and genesis of Mesozoic and Cenozoic basalts in Fujian, China. *Regional Geology of China* **19**, 85–91 (in Chinese with English abstract).

LUCIANI, V., COBIANCHI, M. & JENKYNS, H. C. 2001. Biotic and geochemical response to anoxic events: the Aptian pelagic succession of the Gragano Promontory (southern Italy). *Geological Magazine* **138**, 277–98.

LUCIANI, V., COBIANCHI, M. & JENKYNS, H. C. 2004. Albian high-resolution biostratigraphy and isotope stratigraphy: The Coppa della Nuvola pelagic succession of the Gargano Promontory (Southern Italy). *Eclogae Geologicae Helvetiae* **97**, 77–92.

LUDVIGSON, G. A., JOECKEL, R. M., GONZÁLEZ, L. A., GULBRANSON, E. L., RASBURY, E. T., HUNT, G. J., KIRKLAND, J. I. & MADSEN, S. 2010. Correlation of Aptian–Albian carbon isotope excursions in continental strata of the Cretaceous foreland basin, eastern Utah, U.S.A. *Journal of Sedimentary Research* **80**, 955–74.

MALKOČ, M. & MUTTERLOSE, J. 2010. The early Barremian warm pulse and the late Barremian cooling: a high-resolution geochemical record of the boreal realm. *Palaios* **25**, 14–23.

MÉHAY, S., KELLER, C. E., BERNASCONI, S. M., WEISSERT, H., ERBA, E., BOTTINI, C. & HOCHULI, P. A. 2009. A volcanic CO_2 pulse triggered the Cretaceous Oceanic Anoxic Event 1a and a biocalcification crisis. *Geology* **37**, 819–22.

MENEGATTI, A. P., WEISSERT, H., BROWN, R. S., TYSON, R. V., FARRIMOND, P., STRASSER, A. & CARON, M. 1998. High-resolution $\delta^{13}C$ stratigraphy through the early Aptian 'Livello Selli' of the Alpine Tethys. *Paleoceanography* **13**, 530–45.

MORINAGA, H., INOKUCHI, H. & MIYATA, T. 1999. Late Cretaceous paleomagnetism in Fujian and Guangdong, China. *Earth Science Journal of China University of Geoscience* **24**, 142–4 (in Chinese with English abstract).

MOULLADE, M., KUHNT, W., BERGEN, J. A., MASSE, J.-P. & TRONCHETTI, G. 1998. Correlation of biostratigraphic and stable isotope events in the Aptian historical stratotype of La Bedoule (southeast France). *Comptes Rendus de l'Academie des Sciences, Series IIa, Earth and Planetary Science* **327**, 693–8.

MUTTERLOSE, J., BORNEMANN, A. & HERRLE, J. 2009. The Aptian–Albian cold snap: evidence for 'mid' Cretaceous icehouse interludes. *Neues Jahrbuch für Geologie und Paläontologie, Abhandlungen* **252**, 217–25.

NORDT, L., ATCHLEY, S. & DWORKIN, S. 2002. Paleosol barometer indicates extreme fluctuations in atmospheric CO_2 across the Cretaceous–Tertiary boundary. *Geology* **30**, 703–6.

NORDT, L., ATCHLEY, S. & DWORKIN, S. 2003. Terrestrial evidence for two greenhouse events in the latest Cretaceous. *GSA Today* **13**, 4–9.

OGG, J. G., HINNOV, L. A. & HUANG, C. 2012. Chapter 27– Cretaceous. In *The Geologic Time Scale* (eds F. M. Gradstein, J. G. Ogg, M. Schmitz and G. Ogg), pp. 793–853. Amsterdam: Elsevier Science Ltd.

OKADA, H. 1999. Plume-related sedimentary basins in East Asia during the Cretaceous. *Palaeogeography, Palaeoclimatology, Palaeoecology* **150**, 1–11.

PETRIZZO, M. R., HUBER, B. T., GALE, A. S., BARCHETTA, A. & JENKYNS, H. C. 2012. Abrupt planktic foraminiferal turnover across the Niveau Kilian at Col de Pré-Guittard (Vocontian Basin, southeast France): new criteria for defining the Aptian/Albian boundary. *Newsletters on Stratigraphy* **45**, 55–74.

PGSZ (Petroleum Geological Survey of Zhejiang Province). 1979. Report of Petroleum Geological Investigation to the Jinhua-Quxian basin, Zhejiang province (in Chinese). Zhejiang Bureau of Geology, pp. 128 (in Chinese).

PIRRIE, D., MARSHALL, J. D., DOYLE, P. & RICCARDI, A. C. 2004. Cool early Albian climates; new data from Argentina. *Cretaceous Research* **25**, 27–33.

PODLAHA, O. G., MUTTERLOSE, J. & VEIZER, J. 1998. Preservation of $\delta^{18}O$ and $\delta^{13}C$ in belemnite rostra from the Jurassic/Early Cretaceous successions. *American Journal of Science* **298**, 324–47.

PRICE, G. D. 2003. New constraints upon isotope variation during the early Cretaceous (Barremian–Cenomanian) from the Pacific Ocean. *Geological Magazine* **140**, 513–22.

QUAN, C., SUN, C., SUN, Y. & SUN, G. 2009. High resolution estimates of paleo-CO_2 levels through the Campanian (Late Cretaceous) based on *Ginkgo* cuticles. *Cretaceous Research* **30**, 424–8.

REBOULET, S., RAWSON, P. F., MORENO-BEDMAR, J. A., AGUIRRE-URRETA, M. B., BARRAGAN, R., BOGOMOLOV, Y., COMPANY, M., GONZALEZ-ARREOLA, C., STOYANOVA, V. I., LUKENEDER, A., MATRION, B., MITTA, V., RANDRIANALY, H., VASICEK, Z., BARABOSHKIN, E. J., BERT, D., BERSAC, S., BOGDANOVA, T. N., BULOT, L. G., LATIL, J.-L., MIKHAILOVA, I. A., ROPOLO, P. & SZIVES, O. 2011. Report on the 4th International Meeting of the IUGS Lower Cretaceous Ammonite Working Group, the 'Kilian Group', Dijon, France, 30th August, 2010. *Cretaceous Research* **32**, 786–93.

REN, J. S. 1990. *Tectonic Evolution to Ore-forming of Continental Lithosphere in Eastern China and Adjacent Areas*. Bejing, Science Press, 205 pp (in Chinese with English abstract).

REN, J. S. & CHEN, T. 1989. Tectonic evolution of the continental lithosphere in eastern China and adjacent areas. *Journal of Southeast Asian Earth Science* **3**, 17–27.

RETALLACK, G. J. 2001. A 300 million year record of atmospheric carbon dioxide from fossil plant cuticles. *Nature* **411**, 287–90.

RETALLACK, G. J. 2005. Pedogenic carbonate proxies for amount and seasonality of precipitation in paleosols. *Geology* **33**, 333–6.

RETALLACK, G. J. 2009. Greenhouse crises of the past 300 million years. *Geological Society of American Bulletin* **121**, 1441–55.

ROBINSON, S. A., ANDREWS, J. E., HESSELBO, S. P., RADLEY, J. D., DENNIS, P. F., HARDING, I. C. & ALLEN, P. 2002. Atmospheric pCO_2 and depositional environment from stable-isotope geochemistry of calcrete nodules (Barremian, Lower Cretaceous, Wealden Beds, England). *Journal of the Geological Society, London* **159**, 215–24.

ROBINSON, S. A. & HESSELBO, S. P. 2004. Fossil-wood carbon-isotope stratigraphy of the non-marine Wealden Group (Lower Cretaceous, southern England). *Journal of the Geological Society, London* **161**, 133–45.

ROMANEK, C., GROSSMAN, E. & MORSE, J. 1992. Carbon isotopic fractionation in synthetic aragonite and calcite: effects of temperature and precipitation rate. *Geochimica et Cosmochimica Acta* **56**, 419–30.

ROYER, D. L. 2006. CO_2-forced climate thresholds during the Phanerozoic. *Geochimica et Cosmochimica Acta* **70**, 5665–75, doi: 10.1016/j.gca.2005.11.031.

SCHALLER, M. F., WRIGHT, J. D. & KENT, D. V. 2011. Atmospheric pCO_2 perturbations associated with the central Atlantic magmatic province. *Science* **338**, 1404–9.

SCHLANGER, S. O. & JENKYNS, H. C. 1976. Cretaceous oceanic anoxic events: cause and consequence. *Geologie en Mijnbouw* **55**(34), 179–84.

SHOU, Z. 1995. *Cretaceous volcanic sequences and their Ostracoda fauna in Zhejiang, Fujian and Jiangxi provinces of China*. Beijing: Geological Publishing House, 56 pp. (in Chinese with English abstract).

SHU, L. S., FAURE, M., WANG, B., ZHOU, X. M. & SONG, B. 2008. Late Paleozoic–early Mesozoic geological features of South China: response to the Indosinian collision event in southeast Asia. *Comptes Rendus Geoscience* **340**, 151–65.

SHU, L. S., ZHOU, X. M., DENG, P., WANG, B., JIANG, S. Y., YU, J. H. & ZHAO, X. X. 2009. Mesozoic tectonic evolution of the Southeast China Block: new insights from basin analysis. *Journal of Asian Earth Sciences* **34**, 376–91.

SINNINGHE DAMSTÉ, J. S., KUYPERS, M. M. M., PANCOST, R. D. & SCHOUTEN, S. 2008. The carbon isotopic response of algae, (cyano)bacteria, archaea and higher plants to the late Cenomanian perturbation of the global carbon cycle: insights from biomarkers in black shales from the Cape Verde Basin (DSDP Site 367). *Organic Geochemistry* **39**, 1703–18.

SUN, B., XIAO, L., XIE, S. P., DENG, S., WANG, Y., JIA, H. & TURNER, S. 2007. Quantitative analysis of paleoatmospheric CO_2 level based on stomatal characters of fossil *Ginkgo* from Jurassic to Cretaceous in China. *Acta Geologica Sinica* (English Edition) **81**, 931–39.

TAJIKA, E. 1999. Carbon cycle and climate change during the Cretaceous inferred from a biogeochemical carbon cycle model. *The Island Arc* **8**, 293–303.

TRGZ (THIRD REGIONAL GEOLOGICAL SURVEY OF ZHEJIANG PROVINCE). 1992. *Lithostratigraphy of Zhejiang province*. Wuhan: Press of Chinese Geosciences, pp. 164–5 (in Chinese).

VAHRENKAMP, V. C. 2010. Chemostratigraphy of the Lower Cretaceous Shu'aida Formation: A $\delta^{13}C$ reference profile for the Aptian Stage from the southern neo-Tethys Ocean. In *Barremian–Aptian Stratigraphy and Hydrocarbon Habitat of the Eastern Arabian Plate* (eds F. S. P. van Buchem, M. I. Al-Husseini, F. Maurer & H. J. Droste), pp. 107–37. GeoArabia, Special Publication 4/1.

VAN ACHTERBERGH, E., RYAN, C. G., JACKSON, S. E. & GRIFFIN, W. L. 2001. Data reduction software for LA-ICPMS. In *Laser Ablation-ICP-Mass Spectrometry in the Earth Sciences: Principles and Applications* (ed. P. J. Sylvester), pp. 239–43. Ottawa, Ontario, Mineralogical Association of Canada, Short Course Series 29.

VAN DE SCHOOTBRUGGE, B., FÖLLMI, K. B., BULOT, L. G. & BURNS, S. J. 2000. Paleoceanographic changes during the early Cretaceous (Valanginian–Hauterivian): evidence from oxygen and carbon stable isotopes. *Earth and Planetary Science Letters* **181**, 15–31.

WAGNER, T., HERRLE, J. O., SINNINGHE DAMSTÉ, J. S., SCHOUTEN, S., STÜSSER, I. & HOFMANN, P. 2008. Rapid warming and salinity changes of Cretaceous surface waters in the subtropical North Atlantic. *Geology* **36**, 203–6.

WALLMANN, K. 2001. Controls on the Cretaceous and Cenozoic evolution of seawater composition, atmospheric CO_2 and climate. *Geochimica et Cosmochimica Acta* **18**, 3005–25.

WANG, D.-Z., ZHOU, J.-C., QIU, J.-S. & FAN, H.-H. 2000. Characteristics and petrogenesis of late Mesozoic granitic volcanic-intrusive complexes in southeastern China. *Acta Metallurgica Sinica* **6**, 487–98 (in Chinese with English abstract).

WANG, Y., GUAN, T.-Y, HUANG, G.-F., YU, D.-G. & CHEN, C.-L. 2002. Isotope chronological studies of Late Yanshanian Volcanic Rocks in Northeast Jiangxi Province. *Acta Geoscientia Sinica* **23**, 233–6 (in Chinese with English abstract).

WEISSERT, H. 1989. C-isotope stratigraphy, a monitor of paleoenvironmental change: a case study from the Early Cretaceous. *Surveys in Geophysics* **10**, 1–61.

WEISSERT, H. & CHANNELL, J. E. T. 1989. Tethyan carbonate carbon isotope stratigraphy across the Jurassic–Cretaceous boundary: an indicator of decelerated carbon cycling. *Paleoceanography* **4**, 483–94.

WEISSERT, H. & ERBA, E. 2004. Volcanism, CO_2, and palaeoclimate: a Late Jurassic–Early Cretaceous carbon and oxygen isotope record. *Journal of the Geological Society, London* **161**, 695–702.

WEISSERT, H. & LINI, A. 1991. Ice Age interludes during the time of Cretaceous greenhouse climate? In *Controversies in Modern Geology* (eds D. W. Müller, J. A. McKenzie & H. Weissert), pp. 173–91. New York: Academic Press Limited.

WIGNALL, P. B. 2001. Large igneous provinces and mass extinctions. *Earth-Science Reviews* **53**, 1–33.

WILSON, P. A. & NORRIS, R. D. 2001. Warm tropical ocean surface and global anoxia during the mid-Cretaceous period. *Nature* **412**, 425–9.

WU, J. 1995. Late Early Cretaceous charophytes from the Xinjiang basin, Jiangxi and their stratigraphic significance. *Acta Micropalaeontologica Sinica* **12**(1), 79–87 (in Chinese with English abstract).

WU, J. 2000. A study on the 'Luotang Formation' in the Haogangshan Section of Guixi, Jiangxi. *Journal of Stratigraphy* **24**, 72–7 (in Chinese with English abstract).

XING, G.-F., LU, Q.-D., CHEN, R., ZHANG, Z.-Y., NIE, T.-C., LI, L.-M, HUAN, G.-J. & LIN, M. 2008. Study on the ending time of Late Mesozoic tectonic regime transition in South China: comparing to the Yanshan area in North China. *Acta Geologica Sinica* **82**, 451–63 (in Chinese with English abstract).

YU, X.-Q., SHU, L.-S., DENG, P., WANG, B. & ZHU, F.-P. 2003. The sedimentary features of the Jurassic–Tertiary terrestrial strata in southeast China. *Journal of Stratigraphy* **27**, 254–63 (in Chinese with English abstract).

YU, Y.-W. & XU, B-T. 1999. Stratigraphical sequence and geochronology of the Upper Mesozoic volcanosedimentary rock series in Zhejiang. *Journal of Stratigraphy* **23**, 136–45 (in Chinese with English abstract).

ZAKHAROV, Y. D., BARABOSHKIN, E. Y., WEISSERT, H., MICHAILOVA, I. A., SMYSHLYAEVA, O. P. & SAFRONOV, P. P. 2013. Late Barremian–early Aptian climate of the northern middle latitudes: Stable isotope evidence from bivalve and cephalopod molluscs of the Russian Platform. *Cretaceous Research* **44**, 183–201.

ZHANG, H. 1998. Yanshan Event. *Acta Geologica Sinica* **72**, 103–11 (in Chinese with English abstract).

ZHANG, L. 1987. Discovery of fossils in Guifeng region, Yiyang of Jiangxi province and its significances. *Geology of Jiangxi Province* **1**, 137–9 (in Chinese with English abstract).

ZHENG, F. 1993. Early Cretaceous palynological flora in Xiaoxi basin of Gutian county, Fujian province. *Geology of Fujian* **12**, 210–17 (in Chinese).

ZHU, D.-C., CHUNG, S.-L., MO, X.-X., ZHAO, Z.-D., NIU, Y., SONG, B. & YANG, Y.-H. 2009. The 132 Ma Comei-Bunbury large igneous province: Remnants identified in present-day southeastern Tibet and southwestern Australia. *Geology* **37**, 583–6.

https://doi.org/10.1017/S0016756813000897 Published online by Cambridge University Press